63. Zhang, P. and Hu, H. (2012) Differential glycosylation of α-dystroglycan and proteins other than α-dystroglycan by like-glycosyltransferase. *Glycobiology*, **22**, 235–247.
64. Bao, X., Kobayashi, M., Hatakeyama, S., Angata, K., Gullberg, D., Nakayama, J., Fukuda, M.N. and Fukuda, M. (2009) Tumor suppressor function of laminin-binding α-dystroglycan requires a distinct β3-N-acetylglucosaminyltransferase. *Proc. Natl. Acad. Sci. USA*, **106**, 12109–12114.
65. Yu, M., He, Y., Wang, K., Zhang, P., Zhang, S. and Hu, H. (2013) Adeno-associated viral-mediated LARGE gene therapy rescues the muscular dystrophic phenotype in mouse models of dystroglycanopathy. *Hum. Gene. Ther.*, **24**, 317–330.
66. Saito, F., Masaki, T., Saito, Y., Nakamura, A., Takeda, S., Shimizu, T., Toda, T. and Matsumura, K. (2007) Defective peripheral nerve myelination and neuromuscular junction formation in fukutin-deficient chimeric mice. *J. Neurochem.*, **101**, 1712–1722.

OPEN ACCESS Freely available online

PLOS | ONE

Contribution of Dysferlin Deficiency to Skeletal Muscle Pathology in Asymptomatic and Severe Dystroglycanopathy Models: Generation of a New Model for Fukuyama Congenital Muscular Dystrophy

Motoi Kanagawa[1¶], Zhongpeng Lu[1¶], Chiyomi Ito[1], Chie Matsuda[2], Katsuya Miyake[3], Tatsushi Toda[1]*

1 Division of Neurology/Molecular Brain Science, Kobe University Graduate School of Medicine, Kobe, Japan, **2** Biomedical Research Institute, National Institute of Advanced Industrial Science and Technology, Tsukuba, Japan, **3** Department of Histology and Cell Biology, School of Medicine, Kagawa University, Ikenobe, Miki, Kagawa, Japan

Abstract

Defects in dystroglycan glycosylation are associated with a group of muscular dystrophies, termed dystroglycanopathies, that include Fukuyama congenital muscular dystrophy (FCMD). It is widely believed that abnormal glycosylation of dystroglycan leads to disease-causing membrane fragility. We previously generated knock-in mice carrying a founder retrotransposal insertion in *fukutin*, the gene responsible for FCMD, but these mice did not develop muscular dystrophy, which hindered exploring therapeutic strategies. We hypothesized that dysferlin functions may contribute to muscle cell viability in the knock-in mice; however, pathological interactions between glycosylation abnormalities and dysferlin defects remain unexplored. To investigate contributions of dysferlin deficiency to the pathology of dystroglycanopathy, we have crossed dysferlin-deficient *dysferlin*$^{sjl/sjl}$ mice to the fukutin-knock-in *fukutin*$^{Hp/-}$ and Large-deficient *Large*$^{myd/myd}$ mice, which are phenotypically distinct models of dystroglycanopathy. The *fukutin*$^{Hp/-}$ mice do not show a dystrophic phenotype; however, (*dysferlin*$^{sjl/sjl}$: *fukutin*$^{Hp/-}$) mice showed a deteriorated phenotype compared with (*dysferlin*$^{sjl/sjl}$: *fukutin*$^{Hp/+}$) mice. These data indicate that the absence of functional dysferlin in the asymptomatic *fukutin*$^{Hp/-}$ mice triggers disease manifestation and aggravates the dystrophic phenotype. A series of pathological analyses using double mutant mice for Large and dysferlin indicate that the protective effects of dysferlin appear diminished when the dystrophic pathology is severe and also may depend on the amount of dysferlin proteins. Together, our results show that dysferlin exerts protective effects on the *fukutin*$^{Hp/-}$ FCMD mouse model, and the (*dysferlin*$^{sjl/sjl}$: *fukutin*$^{Hp/-}$) mice will be useful as a novel model for a recently proposed antisense oligonucleotide therapy for FCMD.

Citation: Kanagawa M, Lu Z, Ito C, Matsuda C, Miyake K, et al. (2014) Contribution of Dysferlin Deficiency to Skeletal Muscle Pathology in Asymptomatic and Severe Dystroglycanopathy Models: Generation of a New Model for Fukuyama Congenital Muscular Dystrophy. PLoS ONE 9(9): e106721. doi:10.1371/journal.pone.0106721

Editor: Diego Fraidenraich, Rutgers University -New Jersey Medical School, United States of America

Received March 31, 2014; **Accepted** August 1, 2014; **Published** September 8, 2014

Data Availability: The authors confirm that all data underlying the findings are fully available without restriction. All relevant data are within the paper.

Funding: This work was supported by the Ministry of Health, Labor and Welfare of Japan [Intramural Research Grant for Neurological and Psychiatric Disorders of National Center of Neurology and Psychiatry (23B-5)] to T.T. and C.M. (http://www.mhlw.go.jp/english/index.html); the Ministry of Education, Culture, Sports, Science and Technology of Japan [a Grant-in-Aid for Scientific Research (A) 23249049 to T.T.; a Grant-in-Aid for Young Scientists (A) 24687017 to M.K.; a Grant-in-Aid for Exploratory Research (23659454 to M.K.); and a Grant-in-Aid for Scientific Research on Innovative Areas (Deciphering sugar chain-based signals regulating integrative neuronal functions) 24110508 to M.K.] (http://www.mext.go.jp/english/); a Senri Life Science Foundation grant to M.K. (http://www.senri-life.or.jp/); a Takeda Science Foundation grant to M.K. (http://www.takeda-sci.or.jp/); and a Naito Foundation grant to M.K. (https://www.naito-f.or.jp/jp/index.php). The funders had no role in study design, data collection and analysis, decision to publish, or preparation of the manuscript.

Competing Interests: The authors have declared that no competing interests exist.

* Email: toda@med.kobe-u.ac.jp

¶ These authors are joint first authors on this work.

Introduction

Muscular dystrophies are a heterogeneous group of genetic disorders characterized by the progressive loss of muscle strength and integrity. Several lines of evidence have established that the structural linkage between the muscle extracellular matrix and the cytoskeleton is essential in preventing the progression of muscular dystrophy [1]. The dystrophin-glycoprotein complex (DGC) forms the structural linkage, and mutations in components of this complex cause several forms of muscular dystrophy, including Duchenne and limb-girdle muscular dystrophies (LGMDs) [2]. Within the DGC, α- and β-dystroglycans (DG) act as a molecular bridge between the extracellular matrix and the cytoskeleton. α-DG is a highly glycosylated extracellular subunit that functions as a receptor for extracellular matrix proteins such as laminins. *O*-mannosyl glycosylation and a novel phosphodiester-linked modification of *O*-mannose, termed post-phosphoryl modification, are necessary for α-DG to serve as a functional laminin receptor [3,4]. α-DG is anchored on the plasma membrane through non-covalent interaction with a transmembrane-type β-DG, which in turn binds to the dystrophin-actin cytoskeleton.

Fukuyama congenital muscular dystrophy (FCMD: MIM 253800) is an autosomal recessive disorder characterized by severe

muscular dystrophy, abnormal neuronal migration associated with mental retardation and, frequently, eye abnormalities [5]. We identified *fukutin*, the gene responsible for FCMD, and a 3-kb SINE-VNTR-*Alu* (SVA) retrotransposon insertion into the 3′ UTR of *fukutin* as the founder mutation in FCMD [6]. This insertion causes abnormal splicing that leads to the production of non-functional fukutin protein [7]. The introduction of antisense oligonucleotides that target the splice acceptor and splicing enhancers prevented the pathogenic abnormal splicing by SVA in the cells of FCMD patients as well as model mice that carry the retrotransposal insertion [7]. Point mutations in *fukutin* have been reported in patients both inside and outside Japan, and recent studies have revealed a broad clinical spectrum for fukutin-deficient muscular dystrophies [8]. In FCMD, α-DG is abnormally glycosylated, and its laminin-binding activity is decreased [3]. Several other forms of muscular dystrophy are caused by abnormal glycosylation of α-DG; collectively, these conditions are termed "dystroglycanopathies". More than 10 genes have been identified as causative genes in dystroglycanopathies [9–14], some of which encode products that possess enzyme activities involved in synthesizing *O*-mannosyl sugar chains on α-DG [15–18]. Fukutin, LARGE, and Fukutin-related protein (FKRP) participate in forming the post-phosphoryl moiety [4,19]. Overall, dystroglycanopathy gene products appear to be involved in *O*-mannosyl chain synthesis and post-phosphoryl modification; mutations in these pathways commonly result in abnormal glycosylation of α-DG and reduced ligand-binding activity, disrupting the DG-mediated linkage between the extracellular matrix and the cytoskeleton [2].

Defects in DGC components or α-DG glycosylation disrupt the linkage between the extracellular matrix and the cytoskeleton, thus rendering the sarcolemma more susceptible to contraction-induced damage. This is thought to trigger an increase in intracellular Ca^{2+} concentration, eventually leading to necrosis and myofiber degeneration. Myofibers possess an intrinsic mechanism for repair of damaged membranes, and dysferlin plays a pivotal role in the skeletal muscle membrane repair pathway. In humans, dysferlin deficiency leads to LGMD2B, Miyoshi myopathy or a distal myopathy with anterior tibial onset [20]. Dysferlin-deficient mice show defective membrane repair and also develop muscular dystrophy [21]. Several proteins are known to interact with dysferlin [20], and it is expected that these proteins also participate in membrane repair. For example, mitsugumin 53 (MG53, also known as TRIM72) has been implicated in vesicle trafficking to the damage site during the membrane repair process [22].

We previously described a new FCMD mouse model that carries the retrotransposal insertion in the mouse *fukutin* ortholog [23]. These knock-in mice exhibit hypoglycosylated α-DG but do not develop muscular dystrophy. Therefore, these mice are not suitable for testing effectiveness of the antisense oligonucleotide therapy for FCMD. Although skeletal muscle-selective fukutin conditional knock-out mice, namely MCK-fukutin-cKO and Myf5-fukutin-cKO, show dystrophic phenotype [24], they are not applicable for the examination of the antisense oligonucleotide therapy because they do not possess the retrotransposal insertion. We previously reported that the small amount of normally glycosylated α-DG remaining in the skeletal muscle of the knock-in mice prevents muscular dystrophy [23]. However, it is not clear whether this residual glycosylation alone is sufficient to maintain skeletal muscle membrane integrity. We hypothesized that dysferlin functions compensate for presumed membrane fragility caused by a reduced interaction between α-DG and laminin. Furthermore, the exact contribution of dysferlin and dysferlin-interacting proteins to the pathology of dystroglycanopathy is not known. To investigate this question, we crossed dysferlin-deficient mice with two distinct dystroglycanopathy mouse models and analyzed the resultant phenotypes. In addition, if the double mutant mice carrying the retrotransposal insertion show worse dystrophic phenotype than those of dysferlin mutant mice, they can be the first model for the novel antisense oligonucleotide therapy for FCMD.

Materials and Methods

Animals

Dysferlin-deficient SJL/J mice, a strain with a large deletion in the *Dysf* gene [25], were purchased from Charles River Japan. The transgenic mouse carrying a neo cassette disruption of one *fukutin* allele (*fukutin*$^{+/-}$) [26] and the transgenic knock-in homozygous mutant mouse carrying the retrotransposal insertion in the mouse *fukutin* ortholog (*fukutin*$^{Hp/Hp}$) have been described previously [23]. Genotyping for the *Dysf* mutant allele and the *fukutin* mutant allele was performed as described previously [23,25]. All animal procedures were approved by the Animal Care and Use Committee of Kobe University Graduate School of Medicine (P120202-R2) in accordance with guidelines of Ministry of Education, Culture, Sports, Science and Technology (MEXT) and Japan Society for the Promotion of Science (JSPS). The animals were housed in cages (2–4 mice per cage) with wood-chip bedding in an environmentally controlled room (25°C, 12 h light-dark cycle) and provided food and water *ad libitum* at the animal facility of Kobe University Graduate School of Medicine. Well-trained and skilled researchers and experimental technicians, who have knowledge of methods to prevent unnecessary excessive pain, handled the animals and carried out the experiments. Euthanization was done by cervical dislocation. At sacrifice, the muscles were harvested and snap-frozen in liquid nitrogen (for biochemistry) or in liquid-nitrogen-cooled isopentane (for immunofluorescence and histology). The number and ages of animals used in each experiment is indicated in Figure legends and graphs.

To generate double mutant mice for dysferlin and fukutin deficiency, we crossed dysferlin-deficient SJL/J mice [25] (*dysferlin*$^{sjl/sjl}$; SJL background) with two different lines of *fukutin* mutant mice. One is a transgenic mouse carrying a neo cassette disruption for a single *fukutin* allele (*fukutin*$^{+/-}$; 129-C57BL/6 background) [26] (Fig. 1A, line A). The other is a transgenic knock-in homozygous mutant mouse carrying the retrotransposal insertion in the mouse *fukutin* ortholog [23] (*fukutin*$^{Hp/Hp}$; 129-C57BL/6 background) (Fig. 1A, line B). Heterozygous F1 mice in both lines were intercrossed to obtain the following four genotypes (F2): (*dysferlin*$^{sjl/sjl}$: *fukutin*$^{+/-}$); (*dysferlin*$^{sjl/+}$: *fukutin*$^{+/-}$); (*dysferlin*$^{sjl/+}$: *fukutin*$^{Hp/Hp}$); and (*dysferlin*$^{sjl/sjl}$: *fukutin*$^{Hp/Hp}$). We further crossed (*dysferlin*$^{sjl/sjl}$: *fukutin*$^{+/-}$) with (*dysferlin*$^{sjl/+}$: *fukutin*$^{Hp/Hp}$) mice or (*dysferlin*$^{sjl/+}$: *fukutin*$^{+/-}$) with (*dysferlin*$^{sjl/sjl}$: *fukutin*$^{Hp/Hp}$) mice (Fig. 1A, highlighted with gray) to produce four genotypes (F3): (*dysferlin*$^{sjl/+}$: *fukutin*$^{Hp/+}$); (*dysferlin*$^{sjl/+}$: *fukutin*$^{Hp/-}$); (*dysferlin*$^{sjl/sjl}$: *fukutin*$^{Hp/+}$); and (*dysferlin*$^{sjl/sjl}$: *fukutin*$^{Hp/-}$). To generate double mutant mice for dysferlin and Large deficiency, we crossed dysferlin-deficient SJL/J mice (C57BL/6 backcross 7) with Large-deficient *Large*^{myd} mice (*Large*$^{myd/myd}$; C57BL/6 background) [27,28]. Heterozygous F1 mice were intercrossed and the following four genotypes were used for the analyses (F2): (*dysferlin*$^{sjl/+}$: *Large*$^{myd/+}$); (*dysferlin*$^{sjl/sjl}$: *Large*$^{myd/+}$); (*dysferlin*$^{sjl/+}$: *Large*$^{myd/myd}$); and (*dysferlin*$^{sjl/sjl}$: *Large*$^{myd/myd}$). For more effective breeding, we crossed (*dysferlin*$^{sjl/+}$: *Large*$^{myd/+}$) mice with (*dysferlin*$^{sjl/sjl}$: *Large*$^{myd/+}$) mice (Fig. 1B). (*Dysferlin*$^{+/+}$: *Large*$^{myd/myd}$) mice were obtained from

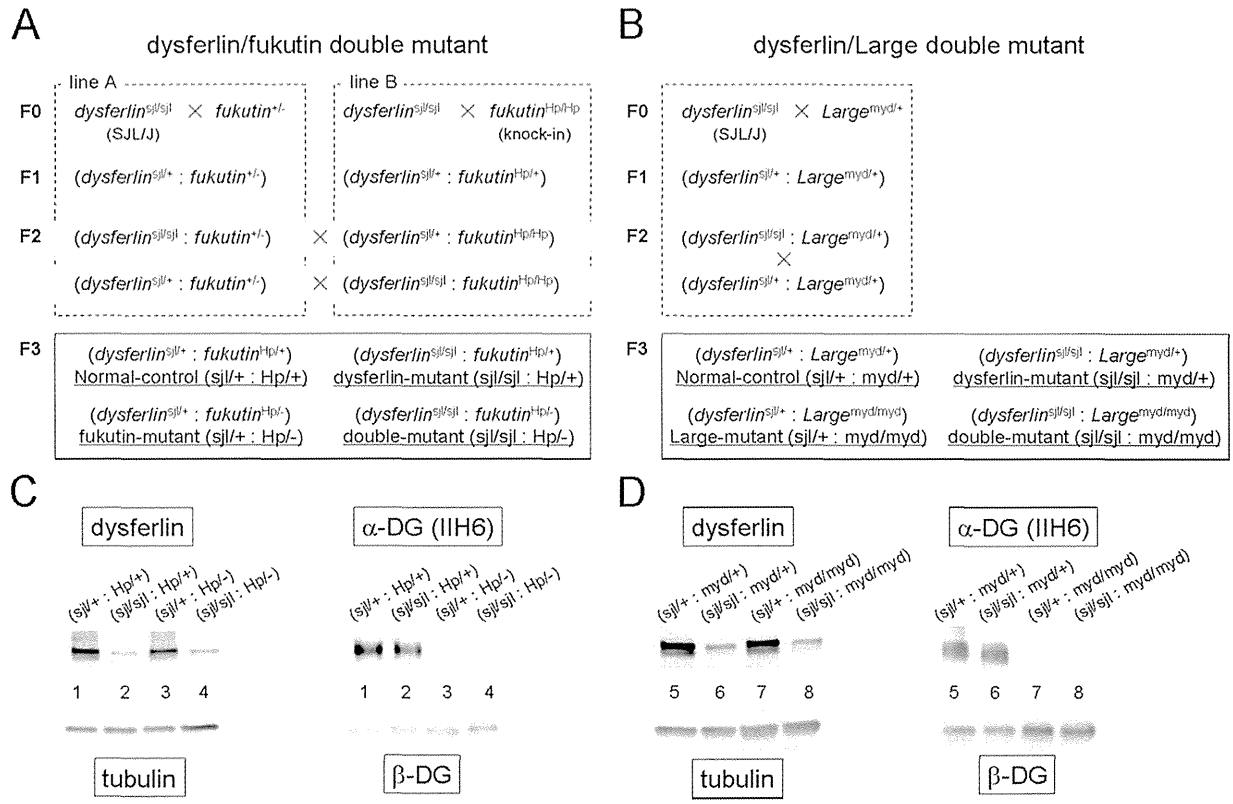

Figure 1. Generation of double-mutant mice exhibiting both abnormal α-DG glycosylation and reduced dysferlin expression. (A, B) Breeding strategy for the generation of double-mutant mice. sjl represents the *dysferlin* mutant allele, myd represents the *Large* mutant allele, and Hp represents the transgenic allele carrying the retrotransposal insertion in *fukutin*. Hp/+ represents a carrier with the insertion in *fukutin*. Hp/− represents a compound heterozygote carrying the insertion and a neo-disrupted allele. For the dysferlin/fukutin double mutant line, we used mice carrying *dysferlin*$^{sjl/+}$ and *fukutin*$^{Hp/+}$ as the normal control (*dysferlin*$^{sjl/+}$: *fukutin*$^{Hp/+}$); *dysferlin*$^{sjl/sjl}$ and *fukutin*$^{Hp/+}$ as the *dysferlin*-mutant (*dysferlin*$^{sjl/sjl}$: *fukutin*$^{Hp/+}$); *dysferlin*$^{sjl/+}$ and *fukutin*$^{Hp/-}$ as the *fukutin*-mutant (*dysferlin*$^{sjl/+}$: *fukutin*$^{Hp/-}$); and *dysferlin*$^{sjl/sjl}$ and *fukutin*$^{Hp/-}$ as the double-mutant (*dysferlin*$^{sjl/sjl}$: *fukutin*$^{Hp/-}$). For the dysferlin/Large double mutant line, we used mice carrying *dysferlin*$^{sjl/+}$ and *Large*$^{myd/+}$ as the normal control (*dysferlin*$^{sjl/+}$: *Large*$^{myd/+}$); *dysferlin*$^{sjl/sjl}$ and *Large*$^{myd/+}$ as the *dysferlin*-mutant (*dysferlin*$^{sjl/sjl}$: *Large*$^{myd/+}$); *dysferlin*$^{sjl/+}$ and *Large*$^{myd/myd}$ as the *Large*-mutant (*dysferlin*$^{sjl/+}$: *Large*$^{myd/myd}$); and *dysferlin*$^{sjl/sjl}$ and *Large*$^{myd/myd}$ as the double mutant (*dysferlin*$^{sjl/sjl}$: *Large*$^{myd/myd}$). (C, D) Abnormal α-DG glycosylation and reduced dysferlin protein expression. Solubilized skeletal muscle samples from each genotype were subjected to Western blot analysis for dysferlin protein expression (left panel). Tubulin was used as a loading control. The solubilized fractions were further enriched for DG by WGA-beads, and the DG-enriched fractions were subjected to Western blotting with the monoclonal IIH6 antibody, which recognizes glycosylated α-DG (right panel). β-DG was used as a loading control. The (*dysferlin*$^{sjl/+}$: *fukutin*$^{Hp/+}$), (*dysferlin*$^{sjl/sjl}$: *fukutin*$^{Hp/+}$), (*dysferlin*$^{sjl/+}$: *fukutin*$^{Hp/-}$), and (*dysferlin*$^{sjl/sjl}$: *fukutin*$^{Hp/-}$) mice are abbreviated as (sjl/+: Hp/+), (sjl/sjl: Hp/+), (sjl/+: Hp/−), and (sjl/sjl: Hp/−), respectively. The (*dysferlin*$^{sjl/+}$: *Large*$^{myd/+}$), (*dysferlin*$^{sjl/sjl}$: *Large*$^{myd/+}$), (*dysferlin*$^{sjl/+}$: *Large*$^{myd/myd}$), and (*dysferlin*$^{sjl/sjl}$: *Large*$^{myd/myd}$) mice are abbreviated as (sjl/+: myd/+), (sjl/sjl: myd/+), (sjl/+: myd/myd), and (sjl/sjl: myd/myd), respectively.
doi:10.1371/journal.pone.0106721.g001

the dysferlin/Large double mutant line and *Large*^{myd} mouse colonies.

Antibodies

Antibodies used in Western blotting and immunofluorescence were as follows: mouse monoclonal antibody 8D5 against β-DG (Novocastra); mouse monoclonal antibody IIH6 against α-DG (Millipore); affinity-purified goat polyclonal antibody against the α-DG core protein (AP-074G-C) [23]; mouse monoclonal antibody NCL-Hamlet against dysferlin (Novocastra); rat monoclonal antibody against mouse F4/80 (BioLegend); rabbit polyclonal antibody against collagen I (AbD serotec); rabbit polyclonal antibody against albumin (DAKO); mouse monoclonal antibody against caveolin-3 (BD Transduction Laboratories); rabbit polyclonal antibody against caveolin-3 (Abcam); and rabbit polyclonal antibody against Trim72 (MG53) (Abcam).

Protein preparation and Western blotting

DG was enriched from solubilized skeletal muscle as described previously [23]. Briefly, skeletal muscles were solubilized in Tris-buffered saline (TBS) containing 1% Triton X-100 and protease inhibitors (Nacalai). The solubilized fraction was incubated with wheat germ agglutinin (WGA)-agarose beads (Vector Laboratories) at 4°C for 16 h, and then DG was eluted with SDS-PAGE loading buffer. For detection of dysferlin and dysferlin-interacting proteins, RIPA buffer (1% NP-40, 0.5% DOC, and 0.1% SDS in TBS with protease inhibitors) was used for protein extraction from skeletal muscle. For this experiment, we used *fukutin*$^{Hp/-}$ mice and litter control *fukutin*$^{Hp/+}$ mice that were backcrossed to C57BL/6 mice more than 10 times. Protein concentration of the solubilized fractions was measured by Lowry methods, using BSA as a standard. Proteins were separated using 3–15% linear gradient SDS-gels. Gels were transferred to polyvinylidene fluoride

(PVDF) membrane (Millipore). Blots were probed with antibodies and then developed with horseradish peroxidase (HRP)-enhanced chemiluminescence (Supersignal West Pico, Pierce; or ECL Plus, GE Healthcare). Protein bands were detected using the LAS-4000 system (Fujifilm), and band intensities were quantified using Multi Gauge V3.2 software (Fujifilm). Statistical analysis was performed with a two-tailed unpaired *t* test. A *p* value of <0.05 was considered to be significant.

Histological and Immunofluorescence analysis

For H&E staining, cryosections (7 μm) were stained for 2 min in hematoxylin, 1 min in eosin, and then dehydrated with ethanol and xylenes. For Masson trichrome staining, sections were fixed with Bouin's solution (Sigma) for 1 hour at 60°C. The slides were incubated in solution A (5% trichloroacetic acid, 5% potassium dichromate) for 30 min, and then stained with Weigert's iron hematoxylin (Muto Chemical Co Ltd) for 15 min. After a rinse with 0.5% HCl in 70% ethanol and a subsequent rinse with warm water, the slides were incubated in solution B (0.5% phosphotungstic acid, 2.5% phosphomolybdic acid) for 1 min, and then stained with FUCHSIN-PONCEAU solution. The slides were washed with 1% acetic acid, incubated in 2.5% phosphomolybdic acid for 5 min, washed with 1% acetic acid, stained with aniline blue, washed with 1% acetic acid, dehydrated, and mounted.

For immunofluorescence analysis, sections were treated with cold ethanol/acetone (1:1) for 1 min, blocked with 5% goat serum in MOM Mouse Ig Blocking Reagent (Vector Laboratories) at room temperature for 1 h, and then incubated with primary antibodies diluted in MOM Diluent (Vector Laboratories) overnight at 4°C. The slides were washed with PBS and incubated with Alexa Fluor 488-conjugated or Alexa Fluor 555-conjugated secondary antibodies (Molecular Probes) at room temperature for 30 min. Permount (Fisher Scientific) and TISSU MOUNT (Shiraimatsu Kikai) were used for H&E staining and immunofluorescence, respectively. Sections were observed under fluorescence microscopy (Leica DMR, Leica Microsystems).

For quantitative evaluation of muscle pathology, the percentages of myofiber with centrally located nuclei were counted for at least 1,000 fibers for each genotype ($n>4$). For evaluation of the F4/80-positive and the collagen I-positive area, the immunofluorescence signal was quantitatively measured using Image J software. Statistical analysis was performed using values represent means with standard deviations, and *p* values <0.05 were considered significant (Student's *t*-test and Mann–Whitney U test).

Results

Generation of double mutant mice exhibiting both abnormal glycosylation of α-DG and dysferlin deficiency

To generate double mutant mice, we crossed dysferlin-deficient SJL/L mice (*dysferlin*$^{sjl/sjl}$) [25] with two distinct dystroglycanopathy models, fukutin-deficient or Large-deficient mice. Previously we reported a transgenic knock-in homozygous mutant mouse carrying the retrotransposal insertion in the mouse *fukutin* ortholog (*fukutin*$^{Hp/Hp}$) [23]. Compound heterozygous mice carrying the retrotransposal insertion and a neo cassette *fukutin* disruption (*fukutin*$^{Hp/-}$) showed more abnormal glycosylation of α-DG than did mice homozygous for the insertion (*fukutin*$^{Hp/Hp}$ mice), although *fukutin*$^{Hp/-}$ mice did show a detectable amount of residual α-DG glycosylation [23]. For the current study, we generated double mutant mice with the (*dysferlin*$^{sjl/sjl}$: *fukutin*$^{Hp/-}$) genotype (Fig. 1A). The other dystroglycanopathy model, Large-deficient *Large*^{myd} mouse (*Large*$^{myd/myd}$) [27,28] show abnormal glycosylation with no detectable amount of properly glycosylated α-DG. The ligand binding activity of α-DG in *Large*$^{myd/myd}$ mice is greatly reduced compared with that in *fukutin*$^{Hp/-}$ mice [23]. Breeding strategies, genotypes, and abbreviations for these double mutant mice and their controls are shown in Figure 1A and 1B.

To confirm reduced protein expression of dysferlin and abnormal glycosylation of α-DG in these mice, we prepared solubilized fractions from skeletal muscle extracts and enriched for α-DG using wheat germ agglutinin (WGA)-agarose beads. Western blot analysis showed a dramatic reduction of dysferlin protein in skeletal muscle from (*dysferlin*$^{sjl/sjl}$: *fukutin*$^{Hp/+}$), (*dysferlin*$^{sjl/sjl}$: *fukutin*$^{Hp/-}$), (*dysferlin*$^{sjl/sjl}$: *Large*$^{myd/+}$), and (*dysferlin*$^{sjl/sjl}$: *Large*$^{myd/myd}$) mice (Fig. 1C and D). We also confirmed a significant reduction of reactivity against the monoclonal antibody IIH6, which recognizes glycosylated epitopes on α-DG that are necessary for laminin binding activity, in (*dysferlin*$^{sjl/+}$: *fukutin*$^{Hp/-}$), (*dysferlin*$^{sjl/sjl}$: *fukutin*$^{Hp/-}$), (*dysferlin*$^{sjl/+}$: *Large*$^{myd/myd}$), and (*dysferlin*$^{sjl/sjl}$: *Large*$^{myd/myd}$) (Fig. 1C and D). Overall, these data confirmed the production of model mice with four biochemically distinct genotypes in each double mutant line.

More severe muscular dystrophy in (*dysferlin*$^{sjl/sjl}$: *fukutin*$^{Hp/-}$) than in (*dysferlin*$^{sjl/sjl}$: *fukutin*$^{Hp/+}$) mice

We examined the histopathology of (*dysferlin*$^{sjl/sjl}$: *fukutin*$^{Hp/-}$) mice by hematoxylin and eosin (H&E) staining. The (*dysferlin*$^{sjl/+}$: *fukutin*$^{Hp/-}$) mice showed no obvious pathological features of muscular dystrophy (Fig. 2). The (*dysferlin*$^{sjl/sjl}$: *fukutin*$^{Hp/+}$) mice showed mild dystrophic changes such as the presence of necrotic fibers and centrally located nuclei (Fig. 2). The phenotypes of (*dysferlin*$^{sjl/+}$: *fukutin*$^{Hp/-}$) and (*dysferlin*$^{sjl/sjl}$: *fukutin*$^{Hp/+}$) mice are similar to those described previously for retrotransposon knock-in *fukutin* mutant mice and dysferlin-deficient SJL/J mice, respectively [23,25]. These results also indicate that disruption of one *dysferlin* or one *fukutin* allele does not affect the phenotype of *fukutin*$^{Hp/-}$ or *dysferlin*$^{sjl/sjl}$ single mutant mice, respectively. H&E staining showed that the (*dysferlin*$^{sjl/sjl}$: *fukutin*$^{Hp/-}$) mice showed further progressed and more severe dystrophic features than did the (*dysferlin*$^{sjl/sjl}$: *fukutin*$^{Hp/+}$) mice in quadriceps (Quad), gastrocnemius (Gast), and tibialis anterior (TA) muscles (Fig. 2A and Fig. 3A). Comparison of the percentage of muscle fibers with centrally located nuclei confirmed a more severe dystrophic phenotype in the (*dysferlin*$^{sjl/sjl}$: *fukutin*$^{Hp/-}$) mice than that in the (*dysferlin*$^{sjl/sjl}$: *fukutin*$^{Hp/+}$) mice (Fig. 2B).

To compare the pathological severity in (*dysferlin*$^{sjl/sjl}$: *fukutin*$^{Hp/-}$) and (*dysferlin*$^{sjl/sjl}$: *fukutin*$^{Hp/+}$) skeletal muscle more precisely, we counted the percentage of muscle fibers (TA) with centrally located nuclei at different ages (Fig. 3A and B). In 8-week-old mice, we observed a few fibers with centrally located nuclei and necrotic fibers in both the (*dysferlin*$^{sjl/sjl}$: *fukutin*$^{Hp/+}$) and the (*dysferlin*$^{sjl/sjl}$: *fukutin*$^{Hp/-}$) mice, but no significant differences were seen between the two (data not shown). At 15 weeks and 30 weeks of age, the (*dysferlin*$^{sjl/sjl}$: *fukutin*$^{Hp/-}$) mice show significantly more fibers with centrally located nuclei than do the (*dysferlin*$^{sjl/sjl}$: *fukutin*$^{Hp/+}$) mice (Fig. 3B). The proportion of fibers with centrally located nuclei in the (*dysferlin*$^{sjl/sjl}$: *fukutin*$^{Hp/-}$) mice increased with age. These results indicate more frequent cycles of muscle cell degeneration and regeneration in the (*dysferlin*$^{sjl/sjl}$: *fukutin*$^{Hp/-}$) mice. We next compared infiltration of macrophage and connective tissue as indicators of disease severity. Immunofluorescence analysis using the monoclonal F4/80 antibody, a marker for macrophages, indicated that macrophage infiltration was increased in (*dysferlin*$^{sjl/sjl}$: *fukutin*$^{Hp/-}$) skeletal muscle compared with (*dysferlin*$^{sjl/sjl}$: *fukutin*$^{Hp/+}$) skeletal

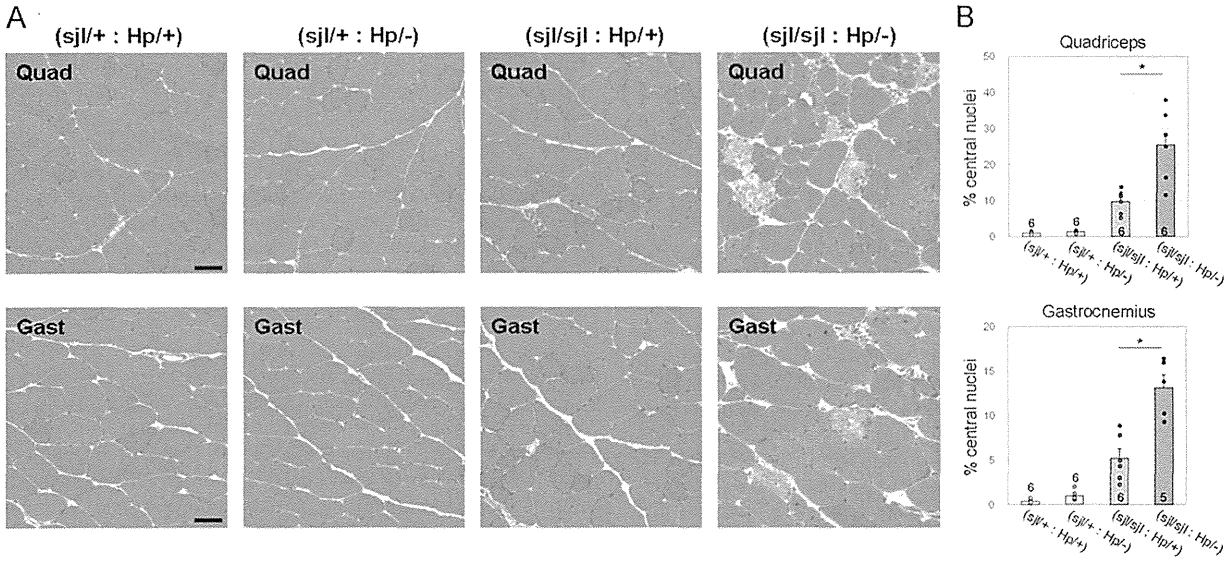

Figure 2. Histological analysis of skeletal muscle from dysferlin/fukutin double mutant mice. (A) Quadriceps (Quad) and gastrocnemius (Gast) muscle tissues from the four mouse genotypes at 15 weeks were analyzed by H&E staining. Bar, 50 μm. (B) Myofibers with centrally located nuclei were counted and quantitatively compared between (*dysferlin*$^{sjl/sjl}$: *fukutin*$^{Hp/+}$) and (*dysferlin*$^{sjl/sjl}$: *fukutin*$^{Hp/-}$) mice (*, $p<0.05$). Data shown are mean ± s.e.m. for each group (*n* is indicated in the graph). The (*dysferlin*$^{sjl/+}$: *fukutin*$^{Hp/+}$), (*dysferlin*$^{sjl/+}$: *fukutin*$^{Hp/-}$), (*dysferlin*$^{sjl/sjl}$: *fukutin*$^{Hp/+}$), and (*dysferlin*$^{sjl/sjl}$: *fukutin*$^{Hp/-}$) mice are abbreviated as (sjl/+: Hp/+), (sjl/+: Hp/−), (sjl/sjl: Hp/+), and (sjl/sjl: Hp/−), respectively.
doi:10.1371/journal.pone.0106721.g002

muscle (Fig. 4A). Quantification of F4/80-immunofluorescence signals confirmed significant increases of macrophage infiltration in (*dysferlin*$^{sjl/sjl}$: *fukutin*$^{Hp/-}$) skeletal muscle (Fig. 4B). Masson trichrome staining revealed that the fibrotic area was increased in (*dysferlin*$^{sjl/sjl}$: *fukutin*$^{Hp/-}$) skeletal muscle (Fig. 4C). Quantification of immunofluorescence signals for collagen I further supported significant increases of connective tissue infiltrations in (*dysferlin*$^{sjl/sjl}$: *fukutin*$^{Hp/-}$) skeletal muscles (Fig. 4D). These data are indicative of further progressed and more severe dystrophic phenotypes in (*dysferlin*$^{sjl/sjl}$: *fukutin*$^{Hp/-}$) skeletal muscle. Importantly, although the (*dysferlin*$^{sjl/+}$: *fukutin*$^{Hp/-}$) mice do not show muscle pathology, the (*dysferlin*$^{sjl/sjl}$: *fukutin*$^{Hp/-}$) mice show a more severe phenotype than do the (*dysferlin*$^{sjl/sjl}$: *fukutin*$^{Hp/+}$) mice, suggesting that dysferlin plays a protective role in preventing disease manifestation in the (*dysferlin*$^{sjl/+}$: *fukutin*$^{Hp/-}$) mice.

Our previous data and those of others suggest that muscle cell membrane fragility due to loss of DG or its functional glycosylation triggers disease manifestation [24,29]. However, we have not observed evidence indicating membrane fragility in *fukutin*$^{Hp/-}$ skeletal muscle [23]. To investigate whether membrane fragility is associated mechanistically with the deteriorated phenotype of the (*dysferlin*$^{sjl/sjl}$: *fukutin*$^{Hp/-}$) mice, we analyzed the population of albumin-positive muscle fibers. Intracellular albumin staining often is used as an indicator of muscle fiber damage or increased membrane permeability [30]. Immunofluorescence analysis suggested that the albumin-positive myofibers were almost absent in both (*dysferlin*$^{sjl/+}$: *fukutin*$^{Hp/+}$) and (*dysferlin*$^{sjl/+}$: *fukutin*$^{Hp/-}$) and only sparsely observed in (*dysferlin*$^{sjl/sjl}$: *fukutin*$^{Hp/+}$) skeletal muscles, whereas they appeared increased in (*dysferlin*$^{sjl/sjl}$: *fukutin*$^{Hp/-}$) skeletal muscle (Fig. 5A). Quantification of albumin-positive fibers also confirmed significant deterioration of the myofiber membrane fragility in the (*dysferlin*$^{sjl/sjl}$: *fukutin*$^{Hp/-}$) mice (Fig. 5B). These data suggest that skeletal muscle fibers in (*dysferlin*$^{sjl/+}$: *fukutin*$^{Hp/-}$) mice have latent membrane fragility, which is protected partially by dysferlin functions, and membrane fragility caused by synergy of reduced α-DG glycosylation and dysferlin-deficiency underlies the deteriorated phenotype of the (*dysferlin*$^{sjl/sjl}$: *fukutin*$^{Hp/-}$) mice.

We examined whether dysferlin itself and/or its interacting proteins, caveolin-3 [31] and MG53 [22], are compensatory upregulated in *fukutin*$^{Hp/-}$ mice. Western blot analysis showed that levels of dysferlin, caveolin-3, and MG53 were not significantly different between *fukutin*$^{Hp/-}$ and *fukutin*$^{Hp/+}$ skeletal muscle (Fig. S1A and B). Immunofluorescence analysis also showed no obvious change in dysferlin expression pattern between *fukutin*$^{Hp/-}$ and *fukutin*$^{Hp/+}$ skeletal muscle (Fig. S1C).

Characterization of muscular dystrophic changes in (*dysferlin*$^{sjl/sjl}$: *Large*$^{myd/myd}$) mice

We subsequently analyzed the histopathology of (*dysferlin*$^{sjl/sjl}$: *Large*$^{myd/myd}$) mice. *Large*$^{myd/myd}$ mice show severe muscular dystrophic phenotypes such as infiltration of connective and fat tissues and marked variation in fiber size [28]. Almost all α-DG is hypoglycosylated in *Large*$^{myd/myd}$ mice [23]. We confirmed that the pathology of (*dysferlin*$^{sjl/+}$: *Large*$^{myd/myd}$) mice was more severe than that in (*dysferlin*$^{sjl/sjl}$: *Large*$^{myd/+}$) mice (Fig. 6). To examine whether the dysferlin functions have protective roles in *Large*$^{myd/myd}$ skeletal muscle, we compared the pathology in (*dysferlin*$^{sjl/+}$: *Large*$^{myd/myd}$) and (*dysferlin*$^{sjl/sjl}$: *Large*$^{myd/myd}$) mice. The (*dysferlin*$^{sjl/+}$: *Large*$^{myd/myd}$) mice showed necrotic and centrally nucleated fibers, indicating frequent cycles of muscle degeneration and regeneration (Fig. 6C). In addition, some animals showed signs of advanced muscular dystrophic changes such as variations in fiber size and connective tissue infiltration (Fig. 6D). The (*dysferlin*$^{sjl/sjl}$: *Large*$^{myd/myd}$) mice exhibited severe pathology, including marked variation in fiber size and large areas with infiltration (Fig. 6E and F). We evaluated these pathologies quantitatively by measuring the areas of macrophage or connective tissue infiltration and the population of albumin-positive

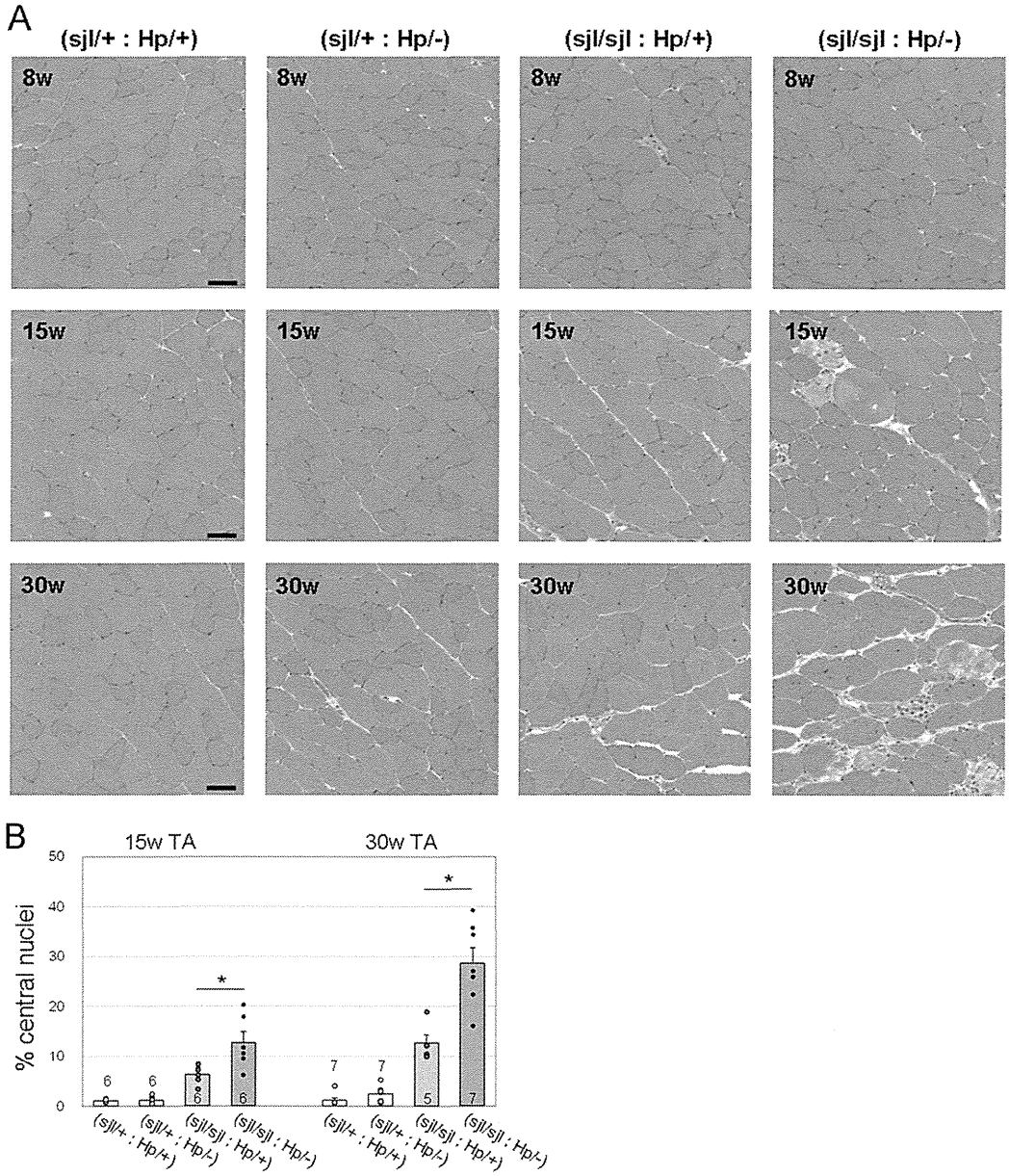

Figure 3. Pathological comparisons between (dysferlin$^{sjl/sjl}$: fukutin$^{Hp/+}$) and (dysferlin$^{sjl/sjl}$ and fukutin$^{Hp/-}$) mice. (A) H&E staining of TA muscle from (*dysferlin*$^{sjl/+}$: *fukutin*$^{Hp/+}$), (*dysferlin*$^{sjl/+}$: *fukutin*$^{Hp/-}$), (*dysferlin*$^{sjl/sjl}$: *fukutin*$^{Hp/+}$) and (*dysferlin*$^{sjl/sjl}$: *fukutin*$^{Hp/-}$) mice at 8, 15 and 30 weeks. Bar, 50 μm. (B) Myofibers with centrally located nuclei were counted and quantitatively compared between (*dysferlin*$^{sjl/sjl}$: *fukutin*$^{Hp/+}$) and (*dysferlin*$^{sjl/sjl}$: *fukutin*$^{Hp/-}$) mice at 15 and 30 weeks (*, $p < 0.05$). Data shown are mean ± s.e.m. for each group (*n* is indicated in the graph). The (*dysferlin*$^{sjl/+}$: *fukutin*$^{Hp/+}$), (*dysferlin*$^{sjl/+}$: *fukutin*$^{Hp/-}$), (*dysferlin*$^{sjl/sjl}$: *fukutin*$^{Hp/+}$), and (*dysferlin*$^{sjl/sjl}$: *fukutin*$^{Hp/-}$) mice are abbreviated as (sjl/+: Hp/+), (sjl/+: Hp/−), (sjl/sjl: Hp/+), and (sjl/sjl: Hp/−), respectively.
doi:10.1371/journal.pone.0106721.g003

muscle fibers (Fig. 6I, J, and K). Both the macrophage-infiltrated area and the population of albumin-positive muscle fibers tended to be larger in (*dysferlin*$^{sjl/sjl}$: *Large*$^{myd/myd}$) than in (*dysferlin*$^{sjl/+}$: *Large*$^{myd/myd}$); however, we did not observe statistically significant differences between the two groups. Furthermore, quantification of collagen I immunofluorescence showed no significant difference in connective tissue infiltration between (*dysferlin*$^{sjl/sjl}$: *Large*$^{myd/myd}$) and (*dysferlin*$^{sjl/+}$: *Large*$^{myd/myd}$) skeletal muscles. These results suggest that dysferlin function produces limited protective effects against the progression of severe muscular dystrophy in *Large*$^{myd/myd}$ mice. Interestingly, however, when compared with the (*dysferlin*$^{+/+}$: *Large*$^{myd/myd}$) mice, the (*dysferlin*$^{sjl/sjl}$: *Large*$^{myd/myd}$) mice showed significant increases in F4/80, collagen I and intracellular albumin staining (Fig. 6I, J, and K). The amount of dysferlin protein in total lysates from (*dysferlin*$^{sjl/sjl}$: *Large*$^{myd/myd}$) and (*dysferlin*$^{sjl/+}$: *Large*$^{myd/myd}$) skeletal muscles was estimated to

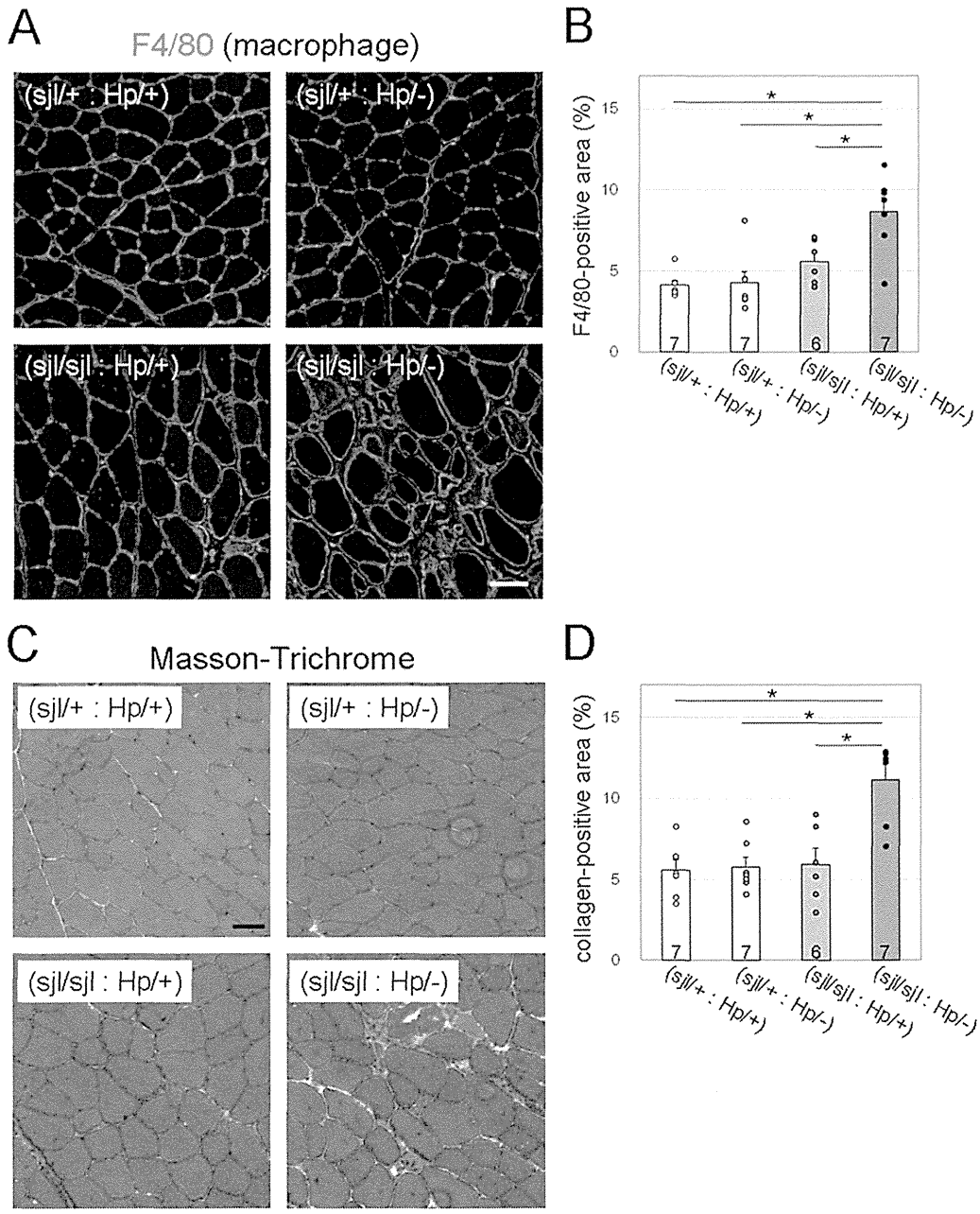

Figure 4. Macrophage and connective tissue infiltration in dysferlin/fukutin double mutant mice. (A) Macrophage infiltration was determined by immunofluorescence analysis using the F4/80 antibody (red). The sarcolemma and nuclei were stained by laminin (green) and DAPI (blue), respectively. TA muscle sections from 30-week-old mice were used. Bar, 50 μm. (B) F4/80-positive immunofluorescence signals were quantified using Image J software. (C) Connective tissue infiltration was determined by Masson-Trichrome staining. TA muscle sections from 30-week-old mice were used. Bar, 50 μm. (D) Quantitative analysis of connective tissue infiltration, determined by immunofluorescence analysis using anti-collagen I antibody. The collagen I-positive area was quantified using Image J software. For quantitative analysis (B and D), data shown are mean ± s.e.m. for each group (*n* is indicated in the graph; *, $p<0.05$). The (*dysferlin*$^{sjl/+}$: *fukutin*$^{Hp/+}$), (*dysferlin*$^{sjl/+}$: *fukutin*$^{Hp/-}$), (*dysferlin*$^{sjl/sjl}$: *fukutin*$^{Hp/+}$), and (*dysferlin*$^{sjl/sjl}$: *fukutin*$^{Hp/-}$) mice are abbreviated as (sjl/+: Hp/+), (sjl/+: Hp/−), (sjl/jl: Hp/+), and (sjl/sjl: Hp/−), respectively.
doi:10.1371/journal.pone.0106721.g004

be ~20% and ~60% of that from (*dysferlin*$^{+/+}$: *Large*$^{myd/myd}$) muscle, respectively (Fig. 6L). These results suggest that the dramatic reduction in the amount/activity of dysferlin protein may be associated with a worse phenotype in the (*dysferlin*$^{sjl/sjl}$: *Large*$^{myd/myd}$) mice. Overall, our results suggest that the protective effects of dysferlin on dystroglycanopathy phenotype appear to be diminished when the dystrophic pathology is severe and progressive and also may depend on the amount of dysferlin proteins.

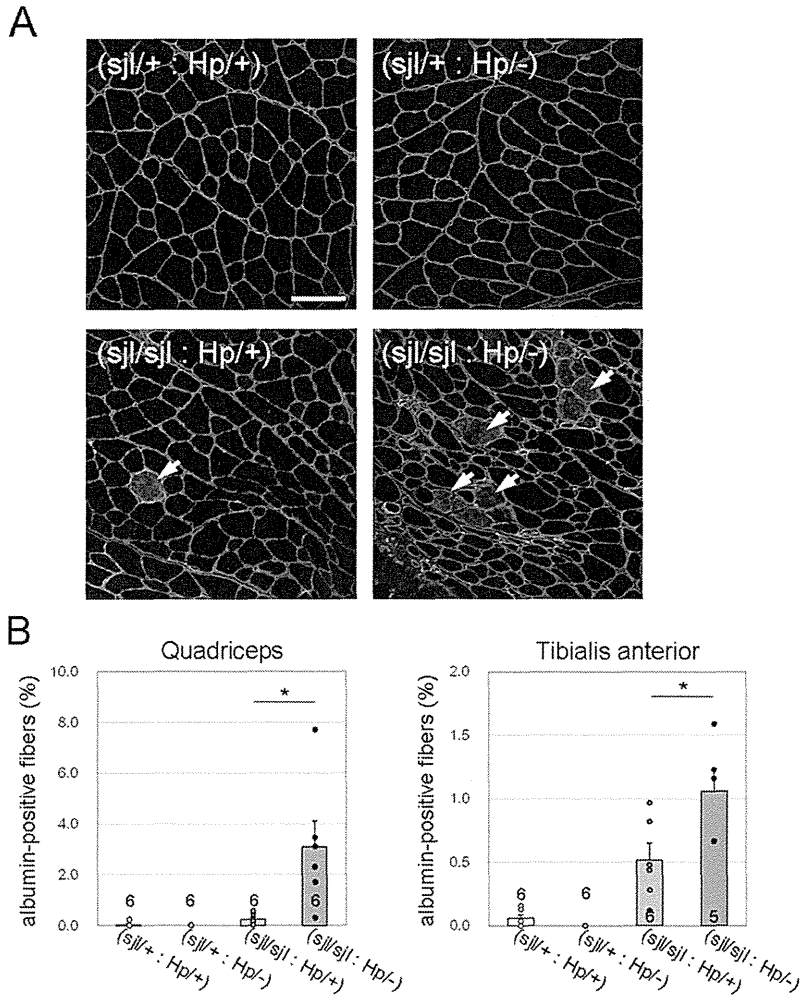

Figure 5. Myofiber membrane fragility in dysferlin/fukutin double mutant mice. (A) Intracellular albumin was determined by immunofluorescence (red). Myofibers are marked by laminin staining (green). Arrows indicate myofibers with intracellular albumin. Images were taken from quadriceps muscle sections of 15-week-old mice. Bar, 100 μm. (B) Myofibers with intracellular albumin were counted and statistically compared between (*dysferlin*$^{sjl/sjl}$: *fukutin*$^{Hp/+}$) and (*dysferlin*$^{sjl/sjl}$: *fukutin*$^{Hp/-}$) mice. Quadriceps and TA muscle sections from 15-week-old mice were analyzed. Data shown are mean ± s.e.m. for each group (*n* is indicated in the graph; *, $p<0.05$). The (*dysferlin*$^{sjl/+}$: *fukutin*$^{Hp/+}$), (*dysferlin*$^{sjl/+}$: *fukutin*$^{Hp/-}$), (*dysferlin*$^{sjl/sjl}$: *fukutin*$^{Hp/+}$), and (*dysferlin*$^{sjl/sjl}$: *fukutin*$^{Hp/-}$) mice are abbreviated as (sjl/+: Hp/+), (sjl/+: Hp/−), (sjl/sjl: Hp/+), and (sjl/sjl: Hp/−), respectively.
doi:10.1371/journal.pone.0106721.g005

Discussion

Here we have characterized the contribution of dysferlin-deficiency to the pathology of dystroglycanopathy using double mutant mice for dysferlin and α-DG glycosylation. To date, several dystroglycanopathy model mice have been established. *Large*^{myd} mice [28] and knock-in mice carrying the FKRP P448L mutation [32] show no detectable amounts of functionally glycosylated α-DG, no laminin binding activity, and progressive muscular dystrophy. On the other hand, other dystroglycanopathy mouse models do not show a muscular dystrophy phenotype [23]. We previously reported that a small amount of intact α-DG in *fukutin*$^{Hp/-}$ mice is sufficient to maintain muscle cell integrity, thus preventing muscular dystrophy [23]. These results and others suggest that the presence of functionally glycosylated α-DG can decrease disease severity [33,34]. In the present study, however, we showed that although (*dysferlin*$^{sjl/+}$: *fukutin*$^{Hp/-}$) mice did not exhibit a muscular dystrophy phenotype, (*dysferlin*$^{sjl/sjl}$: *fukutin*$^{Hp/-}$) mice developed a more exacerbated phenotype than did the *dysferlin* single-mutant (*dysferlin*$^{sjl/sjl}$: *fukutin*$^{Hp/+}$) mice. It has been widely accepted that α-DG glycosylation plays an important role in preventing disease-causing membrane fragility by maintaining a tight association between the basement membrane and the muscle cell membrane, and its defects produce muscle membrane that is susceptible to damage [24,29]. The synergically exacerbated phenotype of the (*dysferlin*$^{sjl/sjl}$: *fukutin*$^{Hp/-}$) mice suggests latent membrane fragility in *fukutin*-deficient *fukutin*$^{Hp/-}$ skeletal muscle. Indeed, the increased number of intracellular albumin-positive fibers in the (*dysferlin*$^{sjl/sjl}$: *fukutin*$^{Hp/-}$) mice also supports this hypothesis. It is assumed in the *fukutin*$^{Hp/-}$ myofiber that interaction between the basement membrane and the cell membrane may be weakened, and therefore disease-causative membrane damage could occur during

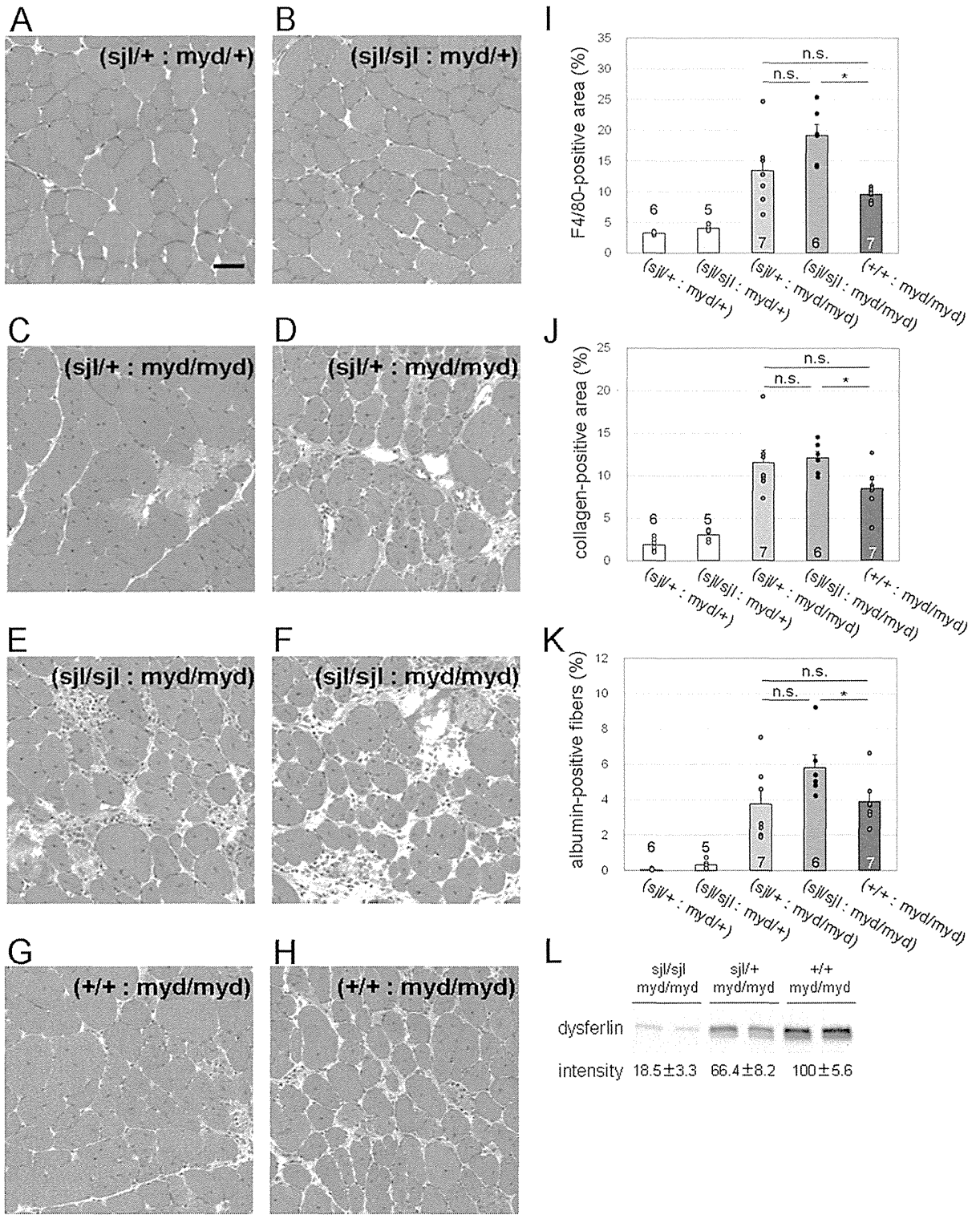

Figure 6. Histopathological analysis of skeletal muscle from dysferlin/Large double mutant mice. (A–H) H&E staining of TA muscle from [(*dysferlin*$^{sjl/+}$: *Large*$^{myd/+}$), A], [(*dysferlin*$^{sjl/sjl}$: *Large*$^{myd/+}$), B], [(*dysferlin*$^{sjl/+}$: *Large*$^{myd/myd}$), C and D], [(*dysferlin*$^{sjl/sjl}$: *Large*$^{myd/myd}$), E and F], and [(*dysferlin*$^{+/+}$: *Large*$^{myd/myd}$), G and H] mice at 15 weeks. Bar, 50 μm. (I) Quantitative analysis of macrophage infiltration, determined by immunofluorescence analysis using F4/80 antibody. (J) Quantitative analysis of connective tissue infiltration determined by immunofluorescence analysis using

anti-collagen I antibody. (K) Quantitative analysis of the proportion of myofibers containing intracellular albumin. For quantitative analysis (I–K), data shown are mean ± s.e.m. for each group (*n* is indicated in the graph; *, $p<0.05$; n.s., not significant). (L) Western blot analysis and quantification of dysferlin expression in the total skeletal muscle lysate from (*dysferlin*$^{sjl/sjl}$: *Large*$^{myd/myd}$), (*dysferlin*$^{sjl/+}$: *Large*$^{myd/myd}$), and (*dysferlin*$^{+/+}$: *Large*$^{myd/myd}$) mice. A representative two individual samples are shown in the blot. Data shown are the average of three individual mice with standard deviations. The (*dysferlin*$^{sjl/+}$: *Large*$^{myd/+}$), (*dysferlin*$^{sjl/sjl}$: *Large*$^{myd/+}$), (*dysferlin*$^{sjl/+}$: *Large*$^{myd/myd}$), (*dysferlin*$^{sjl/sjl}$: *Large*$^{myd/myd}$), and (*dysferlin*$^{+/+}$: *Large*$^{myd/myd}$) mice are abbreviated as (sjl/+: myd/+), (sjl/sjl: myd/+), (sjl/+: myd/myd), (sjl/sjl: myd/myd), and (+/+: myd/myd), respectively.
doi:10.1371/journal.pone.0106721.g006

muscle contractions. However, such presumable membrane fragility may be protected in part by the dysferlin functions.

It is known that dysferlin plays a role in membrane repair pathway and several proteins are known to interact with dysferlin, suggesting that dysferlin forms a protein complex during the membrane repair process. MG53 has been shown to interact with dysferlin and participate in membrane repair, and genetic disruption of MG53 in mice results in muscular dystrophy [22]. Caveolin-3 is known to interact with dysferlin and MG53 [31,35]. In the present study, however, we did not observe compensatory upregulation of these proteins in *fukutin*$^{Hp/-}$ mice, suggesting that dysferlin functions other than membrane repair may play protective roles in the *fukutin*$^{Hp/-}$ mice. Recently, accumulating evidence has suggested new dysferlin roles other than membrane repair, such as T-tubule formation, maintenance, and stabilizing stress-induced Ca^{2+} signaling [36,37]. In addition, it has been reported that dysferlin deficiency leads to increased expression of complement factors and that complement-mediated muscle injury is associated with the pathogenesis of dysferlin-deficient muscular dystrophy [38]. Therefore, it is possible that such impairments independently or synergically contribute to the pathology of the double mutant mice.

Our results showed, rather unexpectedly, that the double-mutant (*dysferlin*$^{sjl/sjl}$: *Large*$^{myd/myd}$) mice did not exhibit significant deterioration of muscle pathology compared with the single-mutant (*dysferlin*$^{sjl/+}$: *Large*$^{myd/myd}$) mice. These data suggest that the protective effects of dysferlin in *Large*$^{myd/myd}$ mice were slightly or much reduced compared with those in *fukutin*$^{Hp/-}$ mice. Since *Large*$^{myd/myd}$ mice showed severe and rapid progressive pathology while *fukutin*$^{Hp/-}$ mice were asymptomatic, our data suggest that the protective effect of dysferlin may be less when disease pathology is advanced and/or severe. It has been reported that a double mutant of dysferlin and dystrophin produced a more exacerbated phenotype than did either single mutant [39]. In our colony, *Large*$^{myd/myd}$ mice show much more severe and rapid progressive pathology than do dystrophin-deficient mdx mice, supporting our hypothesis of a limited protective effect of dysferlin in dystrophic pathology. Interestingly, the (*dysferlin*$^{sjl/sjl}$: *Large*$^{myd/myd}$) mice, however, showed a significantly worse phenotype that did the (*dysferlin*$^{+/+}$: *Large*$^{myd/myd}$) mice. In addition, there is a tendency toward a worse phenotype in the order of dysferlin amount, *i.e.* (*dysferlin*$^{+/+}$: *Large*$^{myd/myd}$), (*dysferlin*$^{sjl/+}$: *Large*$^{myd/myd}$), and (*dysferlin*$^{sjl/sjl}$: *Large*$^{myd/myd}$). These data support the possibility that the protective effect of dysferlin is present even in the severe dystrophic *Large*$^{myd/myd}$ mice. We conclude that dysferlin has the potential to protect muscular dystrophy progression; however, its effect may depend on disease severity and the amount/activity of dysferlin proteins.

Recently, we showed that the retrotransposal insertion in the 3′-UTR region of *fukutin* causes abnormal mRNA splicing, which is induced by a strong splice acceptor site in SVA and a rare alternative donor site in the last exon, to produce an aberrantly spliced fukutin protein [7]. The introduction of antisense oligonucleotides that target the splice acceptor, the predicted exonic splicing enhancer, and the intronic splicing enhancer prevented the pathogenic exon trapping by SVA in the cells of FCMD patients as well as model mice (*fukutin*$^{Hp/Hp}$ and *fukutin*$^{Hp/-}$) [7]. This therapeutic strategy can potentially be applied to almost all FCMD patients in Japan, and can therefore be the first radical clinical treatment for dystroglycanopathies. However, there was no animal model to test the effectiveness of the antisense oligonucleotide therapy. Since *fukutin*$^{Hp/-}$ mice do not exhibit any signs of muscular dystrophy [23], they are not a great model for examining therapeutic effects of this strategy. Skeletal muscle-selective fukutin cKO mice, MCK-fukutin-cKO and Myf5-fukutin-cKO, showed dystrophic pathology [24], but they do not possess the retrotransposal insertion, and thus they are not applicable for testing the antisense oligonucleotide therapy. Our present study demonstrates more severe dystrophic phenotype of (*dysferlin*$^{sjl/sjl}$: *fukutin*$^{Hp/-}$) mice compared with (*dysferlin*$^{sjl/sjl}$: *fukutin*$^{Hp/+}$) mice. Since the (*dysferlin*$^{sjl/sjl}$: *fukutin*$^{Hp/-}$) mice possess the retrotransposal insertion and show dystrophic phenotype, they will be used as the first model for evaluation of the antisense oligonucleotide therapy for FCMD. There is a possibility that the absence of dysferlin could add hurdles on how to interpret the results of the antisense oligonucleotide treatments; however, our quantitative assessments established in this study could overcome this issue. For example, macrophage infiltration (Fig. 4B), connective tissue infiltration (Fig. 4D), and membrane fragility in quadriceps muscles (Fig. 5B) were significantly increased only in the (*dysferlin*$^{sjl/sjl}$: *fukutin*$^{Hp/-}$) mice. These parameters in the (*dysferlin*$^{sjl/sjl}$: *fukutin*$^{Hp/+}$) mice were not changed compared with those in the (*dysferlin*$^{sjl/+}$: *fukutin*$^{Hp/+}$) and the (*dysferlin*$^{sjl/+}$: *fukutin*$^{Hp/-}$) mice, and therefore can be used for quantitative evaluation for therapeutic effects of the antisense oligonucleotide treatments. We hope that generation of this novel FCMD model and establishment of the quantitative evaluation for disease severity will accelerate the future translational researches to overcome FCMD.

Supporting Information

Figure S1 Expression of dysferlin and dysferlin-interacting proteins in *fukutin*$^{Hp/-}$ mice. (A) Western blot analysis of dysferlin, caveolin-3, and MG53 in skeletal muscle extracts from fukutin-deficient *fukutin*$^{Hp/-}$ (Hp/−), and control *fukutin*$^{Hp/+}$ (Hp/+) mice. A representative two individual samples for each mouse line are shown in the blots. (B) Quantification of protein expression (panel A) was shown in graphs. Data shown are the average with standard deviations ($n = 4$ for dysferlin, $n = 3$ for caveolin-3 and MG53). (C) Immunofluorescence analysis of dysferlin in *fukutin*$^{Hp/-}$ (Hp/−) and *fukutin*$^{Hp/+}$ (Hp/+) mice. Bar, 50 μm.
(DOCX)

Acknowledgments

We would like to thank past and present members of the Dr. Toda's laboratory for fruitful discussions and scientific contributions. We also thank Dr. Jennifer Logan for help in editing the manuscript.

Author Contributions

Conceived and designed the experiments: MK ZL TT. Performed the experiments: MK ZL CI KM. Analyzed the data: MK CI. Contributed reagents/materials/analysis tools: CM KM. Contributed to the writing of the manuscript: MK TT.

References

1. Davies KE, Nowak KJ (2006) Molecular mechanisms of muscular dystrophies: old and new players. Nat Rev Mol Cell Biol 7: 762–773.
2. Barresi R, Campbell KP (2006) Dystroglycan: from biosynthesis to pathogenesis of human disease. J Cell Sci 119: 199–207.
3. Michele DE, Barresi R, Kanagawa M, Saito F, Cohn RD, et al. (2002) Post-translational disruption of dystroglycan-ligand interactions in congenital muscular dystrophies. Nature 418: 417–422.
4. Yoshida-Moriguchi T, Yu L, Stalnaker SH, Davis S, Kunz S, et al. (2010) O-mannosyl phosphorylation of alpha-dystroglycan is required for laminin binding. Science 327: 88–92.
5. Fukuyama Y, Osawa M, Suzuki H (1981) Congenital progressive muscular dystrophy of the Fukuyama type - clinical, genetic and pathological considerations. Brain Dev 3: 1–29.
6. Kobayashi K, Nakahori Y, Miyake M, Matsumura K, Kondo-Iida E, et al. (1998) An ancient retrotransposal insertion causes Fukuyama-type congenital muscular dystrophy. Nature 394: 388–392.
7. Taniguchi-Ikeda M, Kobayashi K, Kanagawa M, Yu CC, Mori K, et al. (2011) Pathogenic exon-trapping by SVA retrotransposon and rescue in Fukuyama muscular dystrophy. Nature 478: 127–131.
8. Godfrey C, Clement E, Mein R, Brockington M, Smith J, et al. (2007) Refining genotype phenotype correlations in muscular dystrophies with defective glycosylation of dystroglycan. Brain 130: 2725–2735.
9. Wells L (2013) The O-Mannosylation Pathway: Glycosyltransferases and Proteins Implicated in Congenital Muscular Dystrophy. J Biol Chem 288: 6930–6935.
10. Vuillaumier-Barrot S, Bouchet-Séraphin C, Chelbi M, Devisme L, Quentin S, et al. (2012) Identification of mutations in TMEM5 and ISPD as a cause of severe cobblestone lissencephaly. Am J Hum Genet 91: 1135–1143.
11. Jae LT, Raaben M, Riemersma M, van Beusekom E, Blomen VA, et al. (2013) Deciphering the glycosylome of dystroglycanopathies using haploid screens for lassa virus entry. Science 340: 479–483.
12. Buysse K, Riemersma M, Powell G, van Reeuwijk J, Chitayat D, et al. (2013) Missense mutations in β-1,3-N-acetylglucosaminyltransferase 1 (B3GNT1) cause Walker-Warburg syndrome. Hum Mol Genet 22: 1746–1754.
13. Stevens E, Carss KJ, Cirak S, Foley AR, Torelli S, et al. (2013) Mutations in B3GALNT2 cause congenital muscular dystrophy and hypoglycosylation of α-dystroglycan. Am J Hum Genet 92: 354–365.
14. Carss KJ, Stevens E, Foley AR, Cirak S, Riemersma M, et al. (2013) Mutations in GDP-mannose pyrophosphorylase B cause congenital and limb-girdle muscular dystrophies associated with hypoglycosylation of α-dystroglycan. Am J Hum Genet 93: 29–41.
15. Yoshida A, Kobayashi K, Manya H, Taniguchi K, Kano H, et al. (2001) Muscular dystrophy and neuronal migration disorder caused by mutations in a glycosyltransferase, POMGnT1. Dev Cell 1: 717–724.
16. Manya H, Chiba A, Yoshida A, Wang X, Chiba Y, et al. (2004) Demonstration of mammalian protein O-mannosyltransferase activity: coexpression of POMT1 and POMT2 required for enzymatic activity. Proc Natl Acad Sci USA 101: 500–505.
17. Inamori K, Yoshida-Moriguchi T, Hara Y, Anderson ME, Yu L, et al. (2012) Dystroglycan function requires xylosyl- and glucuronyltransferase activities of LARGE. Science 335: 93–96.
18. Yoshida-Moriguchi T, Willer T, Anderson ME, Venzke D, Whyte T, et al. (2013) SGK196 Is a Glycosylation-Specific O-Mannose Kinase Required for Dystroglycan Function. Science 341: 896–899.
19. Kuga A, Kanagawa M, Sudo A, Chan YM, Tajiri M, et al. (2012) Absence of post-phosphoryl modification in dystroglycanopathy mouse models and wild-type tissues expressing non-laminin binding form of α-dystroglycan. J Biol Chem 287: 9560–9567.
20. Mariano A, Henning A, Han R (2013) Dysferlin-deficient muscular dystrophy and innate immune activation. FEBS J 280: 4165–4176.
21. Bansal D, Miyake K, Vogel SS, Groh S, Chen CC, et al. (2003) Defective membrane repair in dysferlin-deficient muscular dystrophy. Nature 423: 168–172.
22. Cai C, Masumiya H, Weisleder N, Matsuda N, Nishi M, et al. (2009) MG53 nucleates assembly of cell membrane repair machinery. Nat Cell Biol 11: 56–64.
23. Kanagawa M, Nishimoto A, Chiyonobu T, Takeda S, Miyagoe-Suzuki Y, et al. (2009) Residual laminin-binding activity and enhanced dystroglycan glycosylation by LARGE in novel model mice to dystroglycanopathy. Hum Mol Genet 18: 621–631.
24. Kanagawa M, Yu CC, Ito C, Fukada S, Hozoji-Inada M, et al. (2013) Impaired viability of muscle precursor cells in muscular dystrophy with glycosylation defects and amelioration of its severe phenotype by limited gene expression. Hum Mol Genet 22: 3003–3015.
25. Bittner RE, Anderson LV, Burkhardt E, Bashir R, Vafiadaki E, et al. (1999) Dysferlin deletion in SJL mice (SJL-Dysf) defines a natural model for limb girdle muscular dystrophy 2B. Nat Genet 23: 141–142.
26. Kurahashi H, Taniguchi M, Meno C, Taniguchi Y, Takeda S, et al. (2005) Basement membrane fragility underlies embryonic lethality in fukutin-null mice. Neurobiol Dis 19: 208–217.
27. Grewal PK, Holzfeind PJ, Bittner RE, Hewitt JE (2001) Mutant glycosyltransferase and altered glycosylation of alpha-dystroglycan in the myodystrophy mouse. Nat Genet 28: 151–154.
28. Holzfeind PJ, Grewal PK, Reitsamer HA, Kechvar J, Lassmann H, et al. (2002) Skeletal, cardiac and tongue muscle pathology, defective retinal transmission, and neuronal migration defects in the Large(myd) mouse defines a natural model for glycosylation-deficient muscle-eye-brain disorders. Hum Mol Genet 11: 2673–2687.
29. Han R, Kanagawa M, Yoshida-Moriguchi T, Rader EP, Ng RA, et al. (2009) Basal lamina strengthens cell membrane integrity via the laminin G domain-binding motif of alpha-dystroglycan. Proc Natl Acad Sci USA 106: 12573–12579.
30. Straub V, Rafael JA, Chamberlain JS, Campbell KP (1997) Animal models for muscular dystrophy show different patterns of sarcolemmal disruption. J Cell Biol 139: 375–385.
31. Matsuda C, Hayashi YK, Ogawa M, Aoki M, Murayama K, et al. (2001) The sarcolemmal proteins dysferlin and caveolin-3 interact in skeletal muscle. Hum Mol Genet 10: 1761–1766.
32. Chan YM, Keramaris-Vrantsis E, Lidov HG, Norton JH, Zinchenko N, et al. (2010) Fukutin-related protein is essential for mouse muscle, brain and eye development and mutation recapitulates the wide clinical spectrums of dystroglycanopathies. Hum Mol Genet 19: 3995–4006.
33. Wang CH, Chan YM, Tang RH, Xiao B, Lu P, et al. (2011) Post-natal knockdown of fukutin-related protein expression in muscle by long-term RNA interference induces dystrophic pathology. Am J Pathol 178: 261–272.
34. Murakami T, Hayashi YK, Noguchi S, Ogawa M, Nonaka I, et al. (2006) Fukutin gene mutations cause dilated cardiomyopathy with minimal muscle weakness. Ann Neurol 60: 597–602.
35. Cai C, Weisleder N, Ko JK, Komazaki S, Sunada Y, et al. (2009) Membrane repair defects in muscular dystrophy are linked to altered interaction between MG53, caveolin-3, and dysferlin. J Biol Chem 284: 15894–15902.
36. Klinge L, Harris J, Sewry C, Charlton R, Anderson L, et al. (2010) Dysferlin associates with the developing T-tubule system in rodent and human skeletal muscle. Muscle Nerve 41: 166–173.
37. Kerr JP, Ziman AP, Mueller AL, Muriel JM, Kleinhans-Welte E, et al. (2013) Dysferlin stabilizes stress-induced Ca^{2+} signaling in the transverse tubule membrane. Proc Natl Acad Sci USA 110: 20831–20836.
38. Han R, Frett EM, Levy JR, Rader EP, Lueck JD, et al. (2010) Genetic ablation of complement C3 attenuates muscle pathology in dysferlin-deficient mice. J Clin Invest 120: 4366–4374.
39. Han R, Rader EP, Levy JR, Bansal D, Campbell KP (2011) Dystrophin deficiency exacerbates skeletal muscle pathology in dysferlin-null mice. Skelet Muscle 1: 35.

Nagata et al. Orphanet Journal of Rare Diseases 2014, 9:125
http://www.ojrd.com/content/9/1/125

ORPHANET JOURNAL OF RARE DISEASES

RESEARCH Open Access

Japanese founder duplications/triplications involving *BHLHA9* are associated with split-hand/foot malformation with or without long bone deficiency and Gollop-Wolfgang complex

Eiko Nagata[1†], Hiroki Kano[2†], Fumiko Kato[1], Rie Yamaguchi[1], Shinichi Nakashima[1], Shinichiro Takayama[3], Rika Kosaki[4], Hidefumi Tonoki[5], Seiji Mizuno[6], Satoshi Watanabe[7], Koh-ichiro Yoshiura[7], Tomoki Kosho[8], Tomonobu Hasegawa[9], Mamori Kimizuka[10], Atsushi Suzuki[11], Kenji Shimizu[11], Hirofumi Ohashi[11], Nobuhiko Haga[12], Hironao Numabe[13], Emiko Horii[14], Toshiro Nagai[15], Hiroshi Yoshihashi[16], Gen Nishimura[17], Tatsushi Toda[18], Shuji Takada[19], Shigetoshi Yokoyama[19,22], Hiroshi Asahara[19,20], Shinichiro Sano[1,21], Maki Fukami[21], Shiro Ikegawa[2] and Tsutomu Ogata[1*]

Abstract

Background: Limb malformations are rare disorders with high genetic heterogeneity. Although multiple genes/loci have been identified in limb malformations, underlying genetic factors still remain to be determined in most patients.

Methods: This study consisted of 51 Japanese families with split-hand/foot malformation (SHFM), SHFM with long bone deficiency (SHFLD) usually affecting the tibia, or Gollop-Wolfgang complex (GWC) characterized by SHFM and femoral bifurcation. Genetic studies included genomewide array comparative genomic hybridization and exome sequencing, together with standard molecular analyses.

Results: We identified duplications/triplications of a 210,050 bp segment containing *BHLHA9* in 29 SHFM patients, 11 SHFLD patients, two GWC patients, and 22 clinically normal relatives from 27 of the 51 families examined, as well as in 2 of 1,000 Japanese controls. Families with SHFLD- and/or GWC-positive patients were more frequent in triplications than in duplications. The fusion point was identical in all the duplications/triplications and was associated with a 4 bp microhomology. There was no sequence homology around the two breakpoints, whereas rearrangement-associated motifs were abundant around one breakpoint. The rs3951819-*D17S1174* haplotype patterns were variable on the duplicated/triplicated segments. No discernible genetic alteration specific to patients was detected within or around *BHLHA9*, in the known causative SHFM genes, or in the exome.
(Continued on next page)

* Correspondence: tomogata@hama-med.ac.jp
†Equal contributors
[1]Department of Pediatrics, Hamamatsu University School of Medicine, Hamamatsu 431-3192, Japan
Full list of author information is available at the end of the article

(Continued from previous page)

Conclusions: These results indicate that *BHLHA9* overdosage constitutes the most frequent susceptibility factor, with a dosage effect, for a range of limb malformations at least in Japan. Notably, this is the first study revealing the underlying genetic factor for the development of GWC, and demonstrating the presence of triplications involving *BHLHA9*. It is inferred that a Japanese founder duplication was generated through a replication-based mechanism and underwent subsequent triplication and haplotype modification through recombination-based mechanisms, and that the duplications/triplications with various haplotypes were widely spread in Japan primarily via clinically normal carriers and identified via manifesting patients. Furthermore, genotype-phenotype analyses of patients reported in this study and the previous studies imply that clinical variability is ascribed to multiple factors including the size of duplications/triplications as a critical factor.

Keywords: *BHLHA9*, Split-hand/foot malformation, Long bone deficiency, Gollop-Wolfgang complex, Expressivity, Penetrance, Susceptibility, Japanese founder copy number gain

Introduction

Split-hand/foot malformation (SHFM), also known as ectrodactyly, is a rare limb malformation involving the central rays of the autopod [1,2]. It presents with median clefts of the hands and feet, aplasia/hypoplasia of the phalanges, metacarpals, and metatarsals, and syndactyly. SHFM results from failure to maintain the central portion of the apical ectodermal ridge (AER) in the developing autopod [1,2]. SHFM is divided into two forms: a non-syndromic form with limb-confined manifestations and a syndromic form with extra-limb manifestations [2]. Furthermore, non-syndromic SHFM can occur as an isolated abnormality confined to digits (hereafter, SHFM refers to this type) or in association with other limb abnormalities as observed in SHFM with long bone deficiency (SHFLD) usually affecting the tibia and in Gollop-Wolfgang complex (GWC) characterized by femoral bifurcation [1,2]. Both syndromic and non-syndromic forms are associated with wide expressivity and penetrance even among members of a single family and among limbs of a single patient [2].

SHFM and SHFLD are genetically heterogeneous conditions reviewed in ref. [2]. To date, SHFM has been identified in patients with heterozygous deletions or translocations involving the *DLX5–DLX6* locus at 7q21.2–21.3 (SHFM1) [3] (*DLX5* mutations have been detected recently), heterozygous duplications at 10q24 (SHFM3), heterozygous mutations of *TP63* at 3q27 (SHFM4), heterozygous deletions affecting *HOXD* cluster at 2q31 (SHFM5), and biallelic mutations of *WNT10B* at 12q31 (SHFM6); in addition, SHFM2 has been assigned to Xq26 by linkage analyses in a large Pakistani kindred [2]. Similarly, a genomewide linkage analysis in a large consanguineous family has identified two SHFLD susceptibility loci, one at 1q42.2–q43 (SHFLD1) and the other at 6q14.1 (SHFLD2); furthermore, after assignment of another SHFLD locus to 17p13.1–13.3 [4], duplications at 17p13.3 (SHFLD3) have been found in patients with SHFLD reviewed in ref. [2]. However, the GWC locus (loci) remains unknown at present.

The duplications at 17p13.3 identified to date are highly variable in size, and harbor *BHLHA9* as the sole gene within the smallest region of overlap [5-9]. *Bhlha9*/*bhlha9* is expressed in the limb bud mesenchyme underlying the AER in mouse and zebrafish embryos, and *bhlha9* knockdown has resulted in shortening of the pectoral fins in zebrafish [6]. Furthermore, *BHLHA9*-containing duplications have been identified not only in patients with SHFLD but also in those with SHFM and clinically normal family members [4-10]. These findings argue for a critical role of *BHLHA9* duplication in the development of SHFM and SHFLD, with variable expressivity and incomplete penetrance.

In this study, we report on *BHLHA9*-containing duplications/triplications with an identical fusion point and various haplotype patterns that were associated with a range of limb malformations including GWC, and discuss on characteristic clinical findings, genomic basis of Japanese founder copy number gains, and underlying factors for phenotypic variability.

Materials and methods

Patients/subjects

We studied 68 patients with SHFM (n = 55), SHFLD (n = 11), or GWC (n = 2), as well as 60 clinically normal relatives, from 51 Japanese families; the pedigrees of 27 of the 51 families and representative clinical findings are shown in Figure 1. All the probands 1–51 had a normal karyotype. Southern blot analysis for SHFM3 locus had been performed in 28 probands with SHFM, indicating 10q24 duplications in two of them [11]. Clinical features including photographs and roentgenograms of a proband with GWC and his brother with SHFLD (family 23 in Figure 1A) were as described previously [12]. The residencies of families 1–51 were widely distributed throughout Japan.

Ethical approval and samples

This study was approved by the Institutional Review Board Committees of Hamamatsu University School of

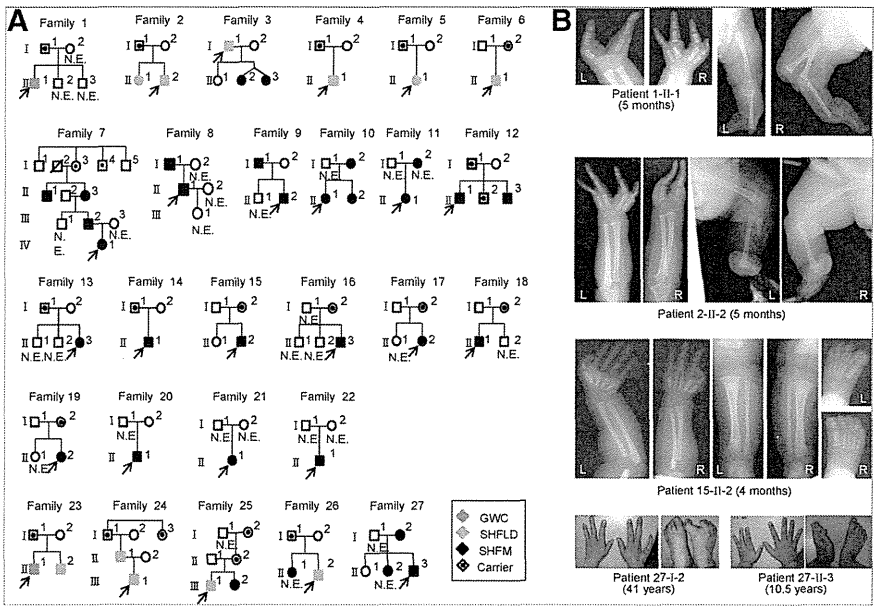

Figure 1 Clinical summary. A. Pedigrees of 27 Japanese families with duplications (families 1–22) and triplications (families 23–27) of a ~200 kb region involving *BHLHA9*. The duplications/triplications are associated with GWC, SHFLD, SHFM, or normal phenotype (carriers). N.E.: Not examined molecularly. **B.** Representative clinical findings. Each patient is indicated by a family-generation-individual style and corresponds to the patient/subject shown in Figure 1A and Additional file 5. The top panel: GWC with right bifid femur; the second panel: SHFLD with bilateral tibial deficiencies, the third panel: SHFM with polydactyly; and the bottom panel: SHFM.

Medicine, RIKEN, and National Center for Child Health and Development, and was performed using peripheral leukocyte samples after obtaining written informed consent for the molecular analysis and the publication of genetic and clinical data after removing information for personal identification (e.g., name, birthday, and facial photograph) from the adult subjects (^{3} 20 years) or from the parents of the child subjects (below 20 years). Furthermore, informed assent was also obtained from child subjects between 6–20 years.

Samples and primers

The primers utilized in this study are summarized in Additional file 1.

Molecular studies

Sanger sequencing, fluorescence *in situ* hybridization (FISH), microsatellite genotyping, Southern blotting, and bisulfite sequencing-based methylation analysis were performed by the standard methods, as reported previously [13]. Quantitative real-time PCR (qPCR) analysis was carried out by the SYBR Green methods on StepOnePlus system, using *RNaseP* as an internal control (Life Technologies). Genomewide oligonucleotide-based array comparative genomic hybridization (CGH) was performed with a catalog human array (4 × 180 K format, ID G4449A) according to the manufacturer's instructions (Agilent Technologies), and obtained copy number variants/polymorphisms were screened with Agilent Genomic Workbench software using the Database of Genomic Variants (http://dgv.tcag.ca/dgv/app/home). Sequencing of a long region encompassing *BHLHA9* was performed with the Nextera XT kit on MiSeq (Illumina), using SAMtools v0.1.17 software (http://samtools.sourceforge.net/). Exome sequencing was performed as described previously [14].

Assessment of genomic environments around the fusion points

Repeat elements around the fusion point were searched for using Repeatmasker (http://www.repeatmasker.org). Rearrangement-inducing DNA features were investigated for 300 bp regions at both the proximal and the distal sides of each breakpoint, using GEECEE (http://emboss.bioinformatics.nl/cgi-bin/emboss/geecee) for calculation of the average GC content, PALINDROME (http://mobyle.pasteur.fr/cgi-bin/portal.py#forms::palindrome) and Non-B DB (http://nonb.abcc.ncifcrf.gov) for the examination of the palindromes and non-B (non-canonical) structures, and Fuzznuc (http://emboss.bioinformatics.nl/cgi-bin/emboss/fuzznuc) for the assessment of rearrangement-associated sequence motifs and tri/tetranucleotides [15-20]. For controls, we examined 48 regions of 600 bp long selected at an interval of 1.5 Mb from the entire chromosome 17.

Statistical analysis

The statistical significance of the frequency was analyzed by the two-sided Fisher's exact probability test.

Results

Sequence analysis of the known causative/candidate genes

We performed direct sequencing for the previously known causative genes (*DLX5*, *TP63*, and *WNT10B*) reviewed in ref. [2] in the probands 1–51. Although no pathologic mutation was identified in *DLX5* and *TP63*, the previously reported homozygous missense mutation of *WNT10B* (c.944C > T, p.R332W) [21] was detected in the proband 48 with SHFM who was born to healthy consanguineous parents heterozygous for this mutation. In addition, while no variation was detected in *DLX5* and *WNT10B*, rs34201045 (4 bp insertion polymorphism) in *TP63* [21] was detected with an allele frequency of 61%.

We also examined *BHLHA9*, because gain-of-function mutations of *BHLHA9* as well as *BHLHA9*-harboring duplications may lead to limb malformations. No sequence variation was identified in the 51 probands.

Array CGH analysis

Array CGH analysis was performed for the probands 1–51, showing increased copy numbers at 17p13.3 encompassing *BHLHA9* (SHFLD3) in the probands 1–27 from families 1–27 (Figure 1A). Furthermore, heterozygous duplications at 10q24 (SHFM3) were detected in the probands 49–51, i.e., a hitherto unreported patient with paternally inherited SHFM (his father also had the duplication) and the two patients who had been indicated to have the duplications by Southern blot analysis [11]. No copy number alteration was observed at other SHFM/SHFLD loci in the probands 1–27 and 49–51. In the remaining probands 28–48, there was no copy number variation that was not registered in the Database of Genomic Variants.

Identical fusion points in *BHLHA9*-containing duplications/triplications

The array CGH indicated that the increased copy number regions at 17p13.3 were quite similar in the physical size in the probands 1–27 and present in three copies in the probands 1–22 and in four copies in the probands 23–27 (Figure 2A). Thus, FISH analysis was performed using 8,259 bp PCR products amplified from this region, showing two signals with a different intensity that was more obvious in the probands 23–27 (Figure 2A).

We next determined the fusion points of the duplications/triplications (Figure 2B). PCR products of 2,195 bp long were obtained with P1/P2 primers in the probands 1–27, and the fusion point was determined by direct sequencing for 418 bp PCR products obtained with P3/P4 primers. The fusion point was identical in all the probands 1–27; it resided on intron 1 of *ABR* and intron 1 of *YWHAE*, and was associated with a 4 bp microhomology.

Then, we performed qPCR analysis for a 214 bp region harboring the fusion point, using P5/P6 primers (Figure 2C and Additional file 2). The fusion point was present in a single copy in the probands 1–22 and in two copies in the probands 23–27. The results showed that the identical genomic segment harboring *BHLHA9* was tandemly duplicated in the probands 1–22 and triplicated in the probands 23–27. According to GRCh37/hg19 (http://genome.ucsc.edu/), the genomic segment was 210,050 bp long.

We also performed array CGH and qPCR for the fusion point in 15 patients other than the probands and 47 clinically normal relatives from the 27 families (Figures 1 and 2C). The duplications/triplications were identified in all the 15 patients. Thus, in a total of 42 patients, duplications/triplications were found in 29 SHFM patients, 11 SHFLD patients, and two GWC patients. Furthermore, the duplications/triplications were also present in 22 of the 47 clinically normal relatives. In particular, they were invariably identified in either of the clinically normal parents when both of them were examined; they were also present in other clinically normal relatives in families 7, 12, 24, and 25.

Since the above data indicated the presence of duplications/triplications in clinically normal subjects, we performed qPCR for the fusion point in 1,000 Japanese controls. The fusion point was detected in a single copy in two subjects (Subjects 1 and 2 in Figure 2C). We also performed array CGH in 200 of the 1,000 controls including the two subjects, confirming the duplications in the two subjects and lack of other copy number variations, including deletions involving *BHLHA9*, which were not registered in the Database of Genomic Variants in the 200 control subjects. The frequency of duplications/triplications was significantly higher in the probands than in the control subjects (27/51 vs. 2/1,000, $P = 3.5 \times 10^{-37}$).

Various haplotype patterns on the duplicated/triplicated segments

We carried out genotyping for rs3951819 (A/G SNP on *BHLHA9*) and *D17S1174* (CA repeat microsatellite locus) on the genomic segment subjected to duplications/triplications (Figure 2A), and determined rs3951819-*D17S1174* haplotype patterns. Representative results are shown in Figure 2D, and all the data are available on request. Various haplotype patterns were identified on the single, the duplicated, and the triplicated segments, and the [A-14] haplotype was most prevalent on the duplicated/triplicated segments (Table 1). While the distribution of CA repeat lengths on the single segments was discontinuous, similar discontinuous distribution was

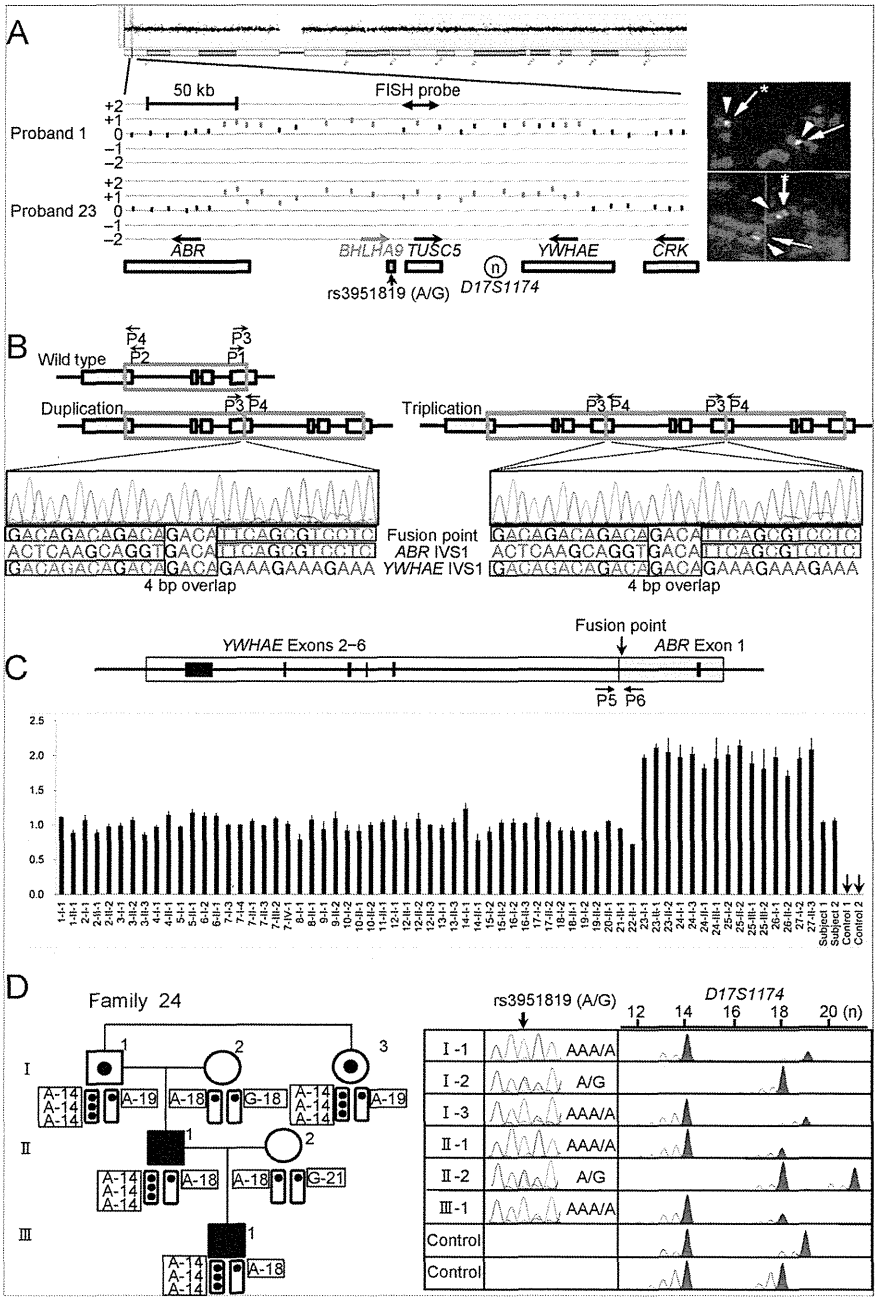

Figure 2 (See legend on next page.)

(See figure on previous page.)
Figure 2 Identification and characterization of the duplications/triplications involving *BHLHA9* at chromosome 17p13.3. A. Array CGH and FISH analyses in proband 1 and proband 23 with GWC. In array CGH analysis, the black and the red dots denote the normal and the increased copy numbers, respectively. Since the log2 signal ratios for a ~200 kb region encompassing *BHLHA9* are around +0.5 in the proband 1 and around +1.0 in the proband 23, this indicates the presence of three and four copies of this region in the two probands, respectively. In FISH analysis, two red signals with an apparently different density are detected by the 8,289 bp PCR probe (the stronger signals are indicated with asterisks). The green signals derive from an internal control probe (CEP17). The arrows on the genes show transcriptional directions. Rs3951819 (A/G) resides within *BHLHA9*. **B**. Determination of the fusion point. The fusion has occurred between intron 1 of *ABR* and intron 1 of *YWHAE*, and is associated with a 4 bp (GACA) microhomology. P1–P4 show the position of primers. **C**. Quantitative real-time PCR analysis. The upper part denotes the fusion point. P5 & P6 show the position of primers. The lower part shows the copy number of the fusion point in patients/subjects with duplications/triplications (indicated by a family-generation-individual style corresponding to that in Figure 1 and Additional file 5). Subject-1 and subject-2 denote the two control subjects with the duplication, and control-1 and control-2 represent normal subjects without the duplication/triplication. **D**. The rs3951819 (A/G SNP)–*D17S1174* (CA repeat number) haplotype patterns in family 24. Assuming no recombination between rs3951819 and *D17S1174*, the haplotype patterns of the family members are determined as shown here. The haplotype patterns of the remaining families have been interpreted similarly.

also observed in the Japanese general population (see Additional file 3).

Genomic environments around the breakpoints

The breakpoint on *YWHAE* intron 1 resided on a simple *Alu* repeat sequence, and that on *ABR* intron 1 was present on a non-repetitive sequence. There was no low copy repeat around the breakpoints. Comparison of the frequencies of known rearrangement-inducing DNA features between 600 bp sequences around the breakpoints and those of 48 regions selected at an interval of 1.5 Mb from chromosome 17 revealed that palindromes, several types of non-B DNA structures, and a rearrangement-associated sequence motif were abundant around the breakpoint on *YWHAE* intron 1 (see Additional file 4).

Clinical findings of families 1–27

Clinical assessment revealed several notable findings. First, duplications/triplications were associated with SHFM, SHFLD, GWC, or normal phenotype, with inter- and intra-familial clinical variability (Figure 1A). Second, in the 42 patients, split hand (SH) was more prevalent than split foot (SF) (41/42 vs. 17/42, $P = 6.2 \times 10^{-9}$), and long bone defect (LBD) was confined to lower extremities (0/42 vs. 13/42, $P = 4.1 \times 10^{-5}$) (Table 2 and Additional file 5). Third, there was no significant sex difference in the ratio between patients with limb malformations and patients/carriers with duplications/triplications (26/38 in males vs. 16/26 in females, $P = 0.60$) (Table 2 and Additional file 5). Fourth, the ratio of LBD positive families was significantly higher in triplications than in duplications (4/5 vs. 16/22, $P = 0.047$) (Figure 1A and Table 2). Fifth, while the duplications/triplications were transmitted from patients to patients, from carriers to patients, and from a carrier to a carrier (from I-1 to II-2 in family 12), transmission from a patient to a carrier was not identified (Figure 1A); it should be pointed out, however, that molecular analysis in a clinically normal child born to an affected parent was possible only in a single adult subject (II-1 in family 27), and that molecular analysis in clinically

Table 1 The rs3951819 (A/G SNP) – *D17S1174* (CA repeat number) haplotype

Patterns of the 210,050 bp segment subjected to copy number gains	
Haplotype pattern	**Family**
<Single segment>	
[A-14]	1, 5, 9, 15, 17, 19, 23, 26
[A-16]	12
[A-18]	3, 14, 15, 24, 25, 26
[A-19]	2, 6, 13, 19, 20, 24, 25, 27
[A-21]	5, 23
[G-12]	17
[G-14]	2, 3, 6, 12, 13, 19, 26
[G-18]	3, 5, 17, 18, 24, 25
[G-19]	9, 12, 18, 20, 25
[G-21]	1, 9, 19, 24, 27
[A-14] or [G-14]	16
[A-18] or [G-18]	4
[A-19] or [G-19]	4
[A-21] or [G-21]	16
<Duplicated segments>	
[A-14] + [A-14]	5, 12, 13, 14, 15, 20
[A-14] + [A-18]	1
[A-14] + [G-18] or [G-14] + [A-18]	2, 3, 4, 6, 9, 16, 17
[A-14] + [G-18] or [A-14] + [G-19]	18
[A-14] + [G-14] or [G-14] + [G-14]	19
<Triplicated segments>	
[A-14] + [A-14] + [A-14]	23, 24
[A-14] + [A-14] + [G-14]	25
[A-14] + [A-19] + [A-19]	26
[A-14] + [G-18] + [G-18] or [G-14] + [A-18] + [G-18]	27

The haplotype patterns written in the left column have been detected in at least one patient/subject in the families described in the right column.
Genotyping could not be performed in several patients/subjects who had been repeatedly examined previously, because of the extremely small amount of DNA samples that were virtually used up in the sequencing and array CGH analyses.

Table 2 Summary of clinical findings in patients/carriers with duplications/triplications involving *BHLHA9*

	SHFM (+) patients			LBD (+) patients			Patient ratio*			LBD (+) families		
	SH	SF	*P*-value	U-LBD	L-LBD	*P*-value	Male	Female	*P*-value	Trip	Dup	*P*-value
This study	41/42	17/42	6.2×10^{-9}	0/42	13/42	4.1×10^{-5}	26/38	16/26	0.60	4/5	16/22	0.047
Previous studies	63/84	23/84	8.6×10^{-10}	11/91	42/91	5.7×10^{-7}	68/114	31/79	5.7×10^{-3}	...	...	...
Sum	104/126	40/126	1.1×10^{-16}	11/133	55/133	3.0×10^{-10}	94/152	47/105	7.6×10^{-3}	...	...	...

SHFM: split-hand/foot malformation; SH: split hand; SF: split foot; LBD: long bone deficiency; U: upper; L: lower; Trip: triplication; and Dup: duplication.
In the previous studies, patients without detailed phenotypic description and those of unknown sex have been excluded (3–9).
*The ratio between patients with limb malformations and patients/carriers with duplications/triplications, i.e. the number of patients over the number of patients plus carriers.

normal children <20 years old was possible only in two subjects (II-2 in family 12 and II-1 in family 15). Lastly, limb malformation was inherited in an apparently autosomal dominant manner (from patients to patients), or took place as an apparently *de novo* event or as an apparently autosomal recessive trait (from clinically normal parents to a single or two affected children) (Figure 1A).

Attempts to identify a possible modifier(s)

The variable expressivity and incomplete penetrance in families 1–27 suggest the presence of a possible modifier (s) for the development of limb malformations. Thus, we performed further molecular studies in patients/subjects in whom DNA samples were still available, and compared the molecular data between patients with SHFM and those with SHFLD for the assessment of variable expressivity and between SHFM, SHFLD, or total patients and carriers for the evaluation of incomplete penetrance.

We first examined the possibility that the modifier(s) resides within or around *BHLHA9* (see Additional file 6). There was no *BHLHA9* mutation in all the 21 examined probands with SHFM, SHFLD, or GWC, as described in the section of "Sequence analysis of the known causative/candidate genes". The rs3951819 A/G SNP pattern on the duplicated/triplicated segments was apparently identical between patients and carriers (e.g. Figure 2D), and the frequency of A/G allele on the normal chromosome 17 was similar between SHFM and SHFLD patients and between SHFM, SHFLD, or total patients and carriers (see Additional file 7). The results of other known SNPs on *BHLHA9* (rs185242872, rs18936498, and rs140504068) were not informative, because of absence or extreme rarity of minor alleles. Furthermore, in SHFM families 7, 12, and 18, sequencing of a 7,406 bp region encompassing *BHLHA9* and Southern blot analysis using five probes and *Mfe*I-, *Ssp*I-, and *Sac*I-digested genomic DNA revealed no variation specific to the patients, and methylation analysis for a CpG rich region at the upstream of *BHLHA9* delineated massive hypomethylation in all the patients/carriers examined.

Next, we examined the possibility that a variant(s) of known causative genes constitutes the modifier(s). Since rs34201045 in *TP63* was identified in the mutation analysis, we compared rs34201045 genotyping data between the 27 probands and the 15 carriers. The allele and genotype frequencies were similar between SHFM and SHFLD patients and between SHFM, SHFLD, or total patients and carriers (see Additional file 8).

We finally performed exome sequencing in SHFM families 13 and 17–19. However, there was no variation specific to the patients. In addition, re-examination of the genomewide array CGH data showed no discernible copy number variation specific to the patients.

Discussion

BHLHA9 overdosage and clinical characteristics

We identified duplications/triplications of a ~ 200 kb genomic segment involving *BHLHA9* at 17p13.3 in 27 of 51 families with SHFM, SHFLD, or GWC. To our knowledge, this is the first study revealing the underlying genetic factor for the development of GWC, and demonstrating the presence of triplications involving *BHLHA9* that were suggested but not confirmed in the previous studies [5,9]. Furthermore, this study indicates that *BHLHA9*-containing duplications/triplications are the most frequent underlying factor for the development of limb malformations at least in Japan. Notably, SHFLD and GWC with LBD were significantly more frequent in patients with triplications than in those with duplications, and the duplications/triplications were identified in clinically normal familial members and in the general population. These findings imply that increased *BHLHA9* copy number constitutes a strong susceptibility, rather than a causative, factor with a dosage effect for the development of a range of limb malformations. Since *Bhlha9* is expressed in the developing ectoderm adjacent to the AER rather than the AER itself in mouse embryos [6], *BHLHA9* appears to play a critical role in the limb development by interacting with the AER. While the duplications/triplications identified in this study included *TUSC5* and generated an *ABR-YWHAE* chimeric gene (Figure 2C), *TUSC5* duplication and the chimeric gene formation are not common findings in the previously reported patients with duplications at 17p13.3 and SHFM and/or SHFLD [5-9]. In addition, none of *Tusc5*, *Abr*, and *Ywhae* is specifically expressed in the developing mouse limb buds [22] (A Transcriptome Atlas Database

for Mouse Embryo of Eurexpress Project, http://www.eurexpress.org/ee/project/).

Several clinical findings are noteworthy in patients/subjects with duplications/triplications. First, SH was more frequent than SF in this study as well as in the previous studies, and LBD was confined to lower extremities in this study and was more frequent in lower extremities than in upper extremities in the previous studies (Table 2) [4-10]. This implies that *BHLHA9* overdosage exerts differential effects on the different parts of limbs. Second, while limb malformations were similarly identified between males and females in this study, they were more frequently observed in males than in females in the previous studies (Table 2) [4-10]. In this regard, it has been reported that testosterone influences the digital growth pattern as indicated by the lower second to fourth digit length ratio in males than in females [23-25], and that Caucasian males have higher serum testosterone values and lower second to fourth digit length ratios than Oriental males [26,27]. Such testosterone effects on the digital growth pattern with ethnic difference may explain why male dominant manifestation was observed in the previous studies primarily from Caucasian countries and was not found in this study. Lastly, LBD was more prevalent in patients with triplications than in those with duplications. This suggests that LBD primarily occurs when the effects of *BHLHA9* overdosage are considerably elevated.

Genomic basis of the Japanese founder copy number gains

The duplications/triplications were associated with the same fusion point and variable haplotype patterns. Since there was no sequence homology or low-copy repeats around the breakpoints, it is unlikely that such duplications/triplications were recurrently produced in different individuals by non-allelic homologous recombination (NAHR) [17,20]. Instead, it is assumed that a Japanese founder duplication took place in a single ancestor, and was spread with subsequent triplication and modification of the haplotype patterns.

The most likely genomic basis of the Japanese duplications/triplications is illustrated in Additional file 9. Notably, a 4 bp (GACA) microhomology was identified at the duplication fusion point (Figure 2B). A microhomology refers to two to five nucleotides common to the sequences of the two breakpoints, and is found as an overlapping sequence at the join point [16,19,20]. This suggests that the Japanese founder duplication was generated by replication-based mechanisms such as fork stalling and template switching (FoSTeS) and microhomology-mediated break-induced replication (MMBIR), because the presence of such a microhomology is characteristic of FoSTeS/MMBIR [17-20]. Indeed, such a simple tandem duplication with a microhomology can be produced by one time FoSTeS/MMBIR [17-20], although it could also be generated by non-homologous end-joining (NHEJ) [17]. Since the [A-14] haplotype was most prevalent on the duplicated/triplicated segments, it is inferred that a genomic rearrangement occurred in an ancestor with the [A-14] haplotype, yielding the founder duplication with the [A-14] + [A-14] haplotype. Furthermore, the presence of multiple stimulants for genomic rearrangements around the breakpoint on *YWHAE* intron 1 would have facilitated the generation of the founder duplication. In particular, non-B structures are known to stimulate the occurrence of both replication-based FoSTeS/MMBIR and double-strand breaks and resultant NHEJ [17,28,29], although the relative importance of each non-B DNA structure is largely unknown.

Subsequent triplication and haplotype modification can develop from the Japanese founder duplication through unequal interchromatid and interchromosomal recombinations [17,20]. Indeed, a tandem triplication with the [A-14] + [A-14] + [A-14] haplotype can be generated by unequal exchange between sister chromatids with the [A-14] + [A-14] haplotype, and various haplotype patterns are yielded by unequal interchromosomal exchanges involving the duplicated or triplicated segments. Furthermore, the haplotype variation would be facilitated by unequal exchanges between sister chromatids harboring duplications/triplications with various haplotype patterns and by the further unequal interchromosomal exchanges.

Underlying factors for the phenotypic variability

The duplications/triplications were accompanied by limb malformations with variable expressivity and incomplete penetrance. Although this may suggest the presence of a possible modifier(s) for the development of limb malformations, such a modifier(s) was not detected. In particular, while patient-to-carrier transmission of duplications/triplications was not identified in this study, even patient-to-carrier-to-patient transmission has been reported in three pedigrees [5,6,10]. Such transmission pattern with incomplete penetrance characterized by skipping of a generation is apparently inexplicable by assuming a modifier (s) interacting with *BHLHA9* or independent of *BHLHA9* on the duplication/triplication positive chromosome 17, on the normal chromosome 17, or on other chromosomes (Figure 3, Models A, B, and C, see also the legends in Figure 3).

In this regard, it is noteworthy that the development of limb malformations is obviously dependent on the size of genomic segment subjected to copy number gains. Actually, limb malformation has occurred in only one of 21 large duplications encompassing *BHLHA9* (average 1.55 Mb, mean 1.12 Mb) and in 29 of 80 small duplications encompassing *BHLHA9* (average 244 kb, mean 263 kb) ($P = 5.9 \times 10^{-3}$) [8]. Consistent with this, the patients with large and